Journal of Plant Growth Regulation
https://doi.org/10.1007/s00344-024-11366-z

Iron-Supplemented Alginate Beads of *Pseudomonas chlororaphis* Improves Charcoal Rot Disease Resistance and the Productivity in Tomato Plants

Amna Shoaib[1] · Huma Shafique[1] · Aneela Anwar[2] · Sidra Javed[1] · Barizah Malik[3] · Samina Mehnaz[4]

Received: 1 November 2023 / Accepted: 12 May 2024

Abstract

Charcoal rot disease, caused by *Macrophomina phaseolina*, poses a major threat to tomatoes. Encapsulating biocontrol bacteria in alginate offers a novel and effective solution with advantages in viability, shelf life, and controlled release. The current research was conducted to develop alginate beads of biocontrol bacteria and to evaluate their inhibitory capacity against *M. phaseolina* in combination with essential metal iron (Fe) using in vitro and in planta tests. In vitro, *Pseudomonas chlororaphis* subsp. *chlororaphis* (PCC-01) exhibited 71% antifungal activity. It also had plant growth-promoting traits of indole-3-acetic acid, hydrogen cyanide, phosphate, and mineral solubilization. FTIR and UV–vis spectra specified good affinity of PCC-01 and alginate, as revealed by changes in the intensity of peaks, particularly at the protein regions (1600–1200 cm^{-1}). The bacterial-loaded alginate beads had excellent properties of encapsulation efficiency (96.20%), swelling ratio (66.47%), moisture content (92.50%), size [1.31 mm (wet) and 0.70 mm (dry)], and ensured slow release of entrapped bacteria up to 120 days. PCA-based biplot, hierarchical clustering, and heat map analysis for in vitro bioassays verified that the antifungal activity of PCC-01-alginate beads improved in nutrient medium supplemented with Fe (91–98%), followed by Mn (74–86%) and Zn (60–76%) via dual culture and modified dual culture methods. In planta, multivariate statistical analyses based on 18 traits related to growth parameters, yield, and biochemical indices of the tomato plants confirmed the greater disease-managing potential of Fe-amended alginate beads of PCC-01 through maximal economic benefits. Therefore, different formulations of PCC-01 and Fe could be prepared and commercialized as a single application product for sustainable and profitable tomato crop production.

Keywords Alginate beads · Biocontrol bacteria · Charcoal rot · Fe

Introduction

Tomato (*Solanum lycopersicum* L.) belongs to the Solanaceae family and is the second-most significant vegetable crop after potatoes with the production of over 189 million tons in 2023. Asia is the leading continent with 63.02% of the global tomato production, followed by Europe, North America, and Africa with 12.94%, 12.52%, and 11.30% of the yield, respectively. Pakistan is ranked at 30th position producing an average yield of 802,151 tons/168,150 ha (Food and Agriculture Organization of the United Nations 2023).

Over 200 diseases can damage tomato plants in the field and after harvest (Kumar et al. 2019). Charcoal rot disease is one of the most serious and devastating crop diseases, damaging crops and minimizing production (Akhtar et al. 2023). It is one of the most important threats to both field

Handling Editor: Wendy Stirk.

✉ Amna Shoaib
amna.iags@pu.edu.pk

[1] Department of Plant Pathology, Faculty of Agricultural Sciences, University of the Punjab, Lahore, Pakistan

[2] Department of Chemistry, University of Engineering and Technology, Lahore, Pakistan

[3] School of Biochemistry & Biotechnology, University of the Punjab, Lahore, Pakistan

[4] Kauser Abdulla Malik School of Life Sciences, Forman Christian College (A Chartered University), Lahore, Pakistan

Published online: 10 June 2024

and greenhouse grown tomatoes in major tomato-growing areas in Pakistan (Hyder et al. 2018). The persistent soil-borne fungus *Macrophomina phaseolina* is the cause of charcoal rot disease that is responsible for a wide spectrum of plant damage, from disruption of physiological function to agricultural yield reduction (Shoaib et al. 2022). Yellow leaves and yellowish to brown stem color that shriveled out to brown are indications of charcoal rot in wilted tomato plants. Black sclerotial bodies with a coarsely shredded appearance are often present in the diseased plants' lower stems (Marquez et al. 2021).

Despite the success rate of certain chemical fumigants (Lokesh et al. 2020), agro-environmental policies and the public's growing aversion to agrochemicals have prompted the evaluation and contrast of chemical agents with alternative methods that are more environmentally friendly to control plant diseases caused by *M. phaseolina* (Adhikary et al. 2019). Biological ways of managing the disease are considered efficient since they do not pose a threat to the environment or inflict harm to humans or animals (Yaqoob et al. 2024). As the fungal genus *Pseudomonas* has antifungal activity and exists in the soil and on the roots of plants, it is potentially appropriate as an inoculant for biofertilization, phytostimulation, and biocontrol (Arrebola et al. 2019). *Pseudomonas chlororaphis*, *P. chlororaphis* subsp. *aurantiaca*, and *P. aurantiaca* have high potential against the phytopathogenic fungus *M. phaseolina* (Rovera et al. 2014). *Pseudomonas* (*P. chlororaphis* subsp. *chlororaphis* and *aurantiaca*) isolated from various plants in Pakistan exhibited antifungal activity, produced secondary metabolites like phenazine-1-carboxylic acid and cyclic lipopeptide (WLIP), and improved growth in the wheat plants (Shahid et al. 2017). Common phenazine derivatives were identified in various strains of both *P. aurantiaca* and *P. chlororaphis*, alongside strain-specific metabolites such as hydrogen cyanide and indole-3-acetic acid, with the corresponding genes documented (Shahid et al. 2021a). The comprehensive findings highlight the potential application of these strains in biofertilizer and biocontrol, supported by a detailed comparative metabolomic analysis of strain-specific metabolites.

In order to successfully implement biocontrol bacteria in field, compatible formulations are required that can ensure the longevity of the biocontrol agents. Formulation containing encapsulated biocontrol agents within alginate is an emerging technique in agriculture, particularly in the management of plant diseases due to its affordability, environmentally friendly, and economical benefits (Riseh et al. 2022). The utilization of biocontrol bacteria in alginate beads permits the controlled release of viable bacterial cells, giving rise to an extended lifespan, greater reproduction potential, and enhanced bacterial cell viability (Rojas-Padilla et al. 2022). For example, stable preparation of alginate microcapsules of rhizobia (*Mesorhizobium ciceri* and *Bradyrhizobium japonicum*) protected bacteria against ultraviolet and other adverse effects and enhanced bacteria viability. The microcapsule of bacteria improved formation of nodules on the roots of chickpea and soybean in field condition (Shcherbakova et al. 2018). Spherical alginate nanoformulation of *Bacillus velezensis* managed 96.33% of bean disease caused by *Rhizoctonia solani* on beans (Moradi-Pour et al. 2022). Calcium alginate microbeads of three beneficial *Bacillus strains* had a high yield/gram for all bacteria, greater survival rates within beads, 75% rate of swelling, and effective release in the soil, which enhanced wheat plant growth (Rojas-Padilla et al. 2022). Encapsulation of bacteria (*Pseudomonas cedrina* subsp. *fulgida*, *P. putida*, and *Klebsiella* sp.) in alginate beads sustained survival rates and the physiological activity of the bacteria, together with stimulation of plant growth (Tirry et al. 2022). Microencapsulation of a *P. chlororaphis* in alginate-whey protein-carbon nanotubes facilitated their controlled release, improved the stability and efficiency of probiotic bacteria, retained their biocontrol properties, and led to their gradual and controlled release (Fathi et al. 2021).

The antifungal potential of the biocontrol bacteria can be improved by combining them with essential metals. Biological bacterial agents have tremendous potential to augment crop production in the presence of essential metals. Iron (Fe) is an important micronutrient that needs to be supplied to nearly all plant species as it has roles in metabolicprocesses such as photosynthesis, DNA synthesis, and respiration (Rout and Sahoo 2015). It functions as a cofactor for multiple enzymes and is necessary for oxygen metabolic processes, electron transport, the tricarboxylic acid cycle, lipid metabolism, and peroxide detoxification (Ma et al. 2015). Iron triggers multiple processes related to metabolism and is a functional group component of many enzymes. It participates in various physiological and metabolic functions in plants. It is vital for an extensive variety of biological processes because it is a precursor of multiple key enzymes, such as cytochromes of the electron transport chain. Fe also takes part in the synthesis of chlorophyll and is needed for the ongoing maintenance of chloroplast form and function (Schmidt et al. 2020).

The application of Fe-amended alginate beads of biocontrol bacteria may represent an affordable and environmentally friendly approach for treating charcoal rot disease in tomato plants. Therefore, the key objective of this study was to investigate the management of the charcoal rot disease of tomato plants by employing Fe-amended microcapsules of alginated rhizobacteria.

Materials and Methods

Assessing Pathogenicity of *Macrophomina phaseolina*

The working culture of the fungal pathogen, viz., *M. phaseolina* (GenBankAccessions MH999811), was previously identified by Siddique et al. (2021). It was grown on 2% Malt extract agar medium (MEA: 2 g Malt extract and 2 g agar in 100 mL autoclaved distilled water) at 30 °C. To confirm the pathogenicity of *M. phaseolina*, healthy tomato fruits were washed and surface-sterilized with a 1% sodium hypochlorite solution for 2 min, followed by three rinses with sterile distilled water. Using a sterilized needle, 2-mm-deep wounds were created on the fruit surface. Each wound received 10 µL sclerotial suspension (10–12 sclerotia) and the control fruits were inoculated with sterile distilled water (10 µL). The inoculated as well as control fruits were kept in plastic polythene bags at 30 °C for 7 days. There were four replicate of each set, and the experiments were conducted in triplicates (Rizwana et al. 2021). Tomato disease severity (DS) was evaluated (Table 1; Safari et al. 2022) and the DS scores were used to calculate the disease severity index (DSI%) using the following equation.

$$\textbf{DSI}\ (\%) = \sum \left(\frac{\textbf{Severity rating} \times \textbf{Number of tomato fruits in the rating}}{\textbf{Total number of tomato fruits used in the rating} \times \textbf{Maximal DS score}} \right) \times \mathbf{100}.$$

Lesion samples were aseptically transferred onto 2% MEA, incubated at 30 °C for 7 days, and observed for colony characteristics (color and texture) and microscopic structures (hyphae and sclerotia) to confirm Koch's postulates.

Screening of Potential Bacterial Strain Against *M. phaseolina*

The dual culture technique was adopted to evaluate in vitro antifungal activity of four bacterial strains against *M. phaseolina* (Table 2). A mycelial disc (5 mm) was taken from a fresh cultured plate of the fungus and placed at one half of the MEA-filled Petri plate (diameter 90 mm × height 15 mm). A single loop of bacterial strain (10^7 to 10^8 colony-forming units (CFUs) per milliliter) from an overnight culture was streaked on the other half of the plate. In the control, only a fungal disc was inoculated on MEA plates. Plates in replicates ($n = 4$) were incubated at 30 °C. After 6 days of incubation, the antagonistic activity of the bacterial strain was determined through a comparison of the diameter of the *M. phaseolina* colony (C) to the antagonist colony (T). The fungal suppression rate was equal to the length of mycelial growth after inhibition compared to that without inhibition using the following formula.

$$\text{Inhibition rate } (\%) = ((C - T)/C) \times 100.$$

P. chlororaphis subsp. *chlororaphis* (PCC-01) interacted with the fungus significantly and was selected for further study as a potential antifungal agent against *M. phaseolina*.

Evaluation of PCC-01 for Plant Growth-Promoting Traits

The PCC-01 was evaluated for their plant growth-promoting traits including hydrogen cyanide (HCN), indole-3-acetic acid (IAA), phosphate solubilizing activity (PSA), and Fe

Table 1 Disease severity score of disease assessment on tomato fruit

Disease score	Description	Interference
0	No visible symptoms on fruit	No infection
1	1–25% of the fruit is covered by slight necrotic and fungal mycelial	Mild infection
2	26–50% of the fruit is covered by slight necrotic and fungal mycelial	Moderate infection
3	51–75% of the area is covered by slight necrotic and fungal mycelial	Severe infection
4	> 76% necrotic tissue with fungal mass and fruit appears soft and decayed	Very severe/devastating

Table 2 Plant bacterial strains employed in the present research

Strains		Accession number
1	*Pseudomonas chlororaphis* subsp. *chlororaphis*	PCC-01 (cotton) (Shahid et al. 2017)
2	*Bacillus amyloliquefaciens*	BA-01 (sugarcane) (Shahid et al. 2021b)
3	*Pseudomonas chlororaphis* subsp. *aurantiaca*	PCA-02 (sugarcane) (Shahid et al. 2017)
4	*Pseudomonas aurantiaca*	PA-03 (para grass) (Shahid et al. 2017)

solubilization tests. To detect HCN formation, PCC-01 was streaked on a nutrient agar medium with 4.4 g/L glycine. A sterilized filter paper, wetted in 1% sodium carbonate and 0.5% picric acid, was placed under the Petri plate lid. After sealing with parafilm, plates were incubated at 28 °C for 72 h. Hydrogen cyanide production was assessed by observing a color change in the filter paper from yellow to reddish-brown (Nithyapriya et al. 2021). For IAA production assay, PCC-01 was cultured in nutrient broth at 27 °C for 24 h in a shaker incubator. Subsequently, 50 µL bacterial suspension was added to nutrient broth supplemented with 50 µg mL^{-1} tryptophan. After 72 h, the suspension was centrifuged, and 2 mL supernatant was mixed with 4 mL of Salkowski reagent (98 mL 35% $HClO_4$ + 2 mL 0.5 M $FeCl_3$). The pink color's intensity was measured at 530 nm (Patten and Glick 1996). For PSA, the bacteria were spot inoculated on Pikovskaya agar [10 g glucose, 0.2 g KCl, 0.5 g $MnSO_4$. $7H_2O$, 0.2 g NaCl, 0.1 g $MgSO_4.7H_2O$, 0.1 g $CaCl_2$ $2H_2O$, 0.5 g $(NH_4)_2SO_4$, 0.5 g $FeSO_4$. $7H_2O$, 5 g $Ca_3(PO_4)_2$, and 15 g agar in 1 L distilled water (pH = 7.5)]. After 4 days of incubation at 28 °C, the plates were tested for the presentation of colorless halos (Patten and Glick 1996). The culture supernatant of PCC-01 was mixed with freshly prepared 0.5 mL 2% aqueous iron sulfate ($FeSO_4$) and observed for the presence and absence of pink color after 30 min for Fe solubilization (Kotasthane et al. 2017).

Preparation and Characterization of Alginate Beads of PCC-01

The method described by Riaz et al. (2023) was used to prepare alginate beads of PCC-01. Briefly, bacterial pellets ($OD_{600} = 2.5–2.8$; 2.0×10^9 to 2.2×10^9 cells/mL) were mixed with phosphate buffer saline and pre-sterilized sodium alginate solution (2%) and iron sulfate (0.0005%) for the preparation of bacterial beads (Fig. 1). The homogenized solution was added drop by drop using a 5-mL sterile syringe in $CaCl_2$ (3%) solution while being stirred magnetically. The freshly formed alginate beads of bacteria (30–35 g) were harvested by filtering through filter paper (Whatman No. 1) and used for further experimentation. There was 1.94×10^9 to 2.1×10^9 cells/mL (70–80 beads) in one g of bacterial beads.

FTIR and UV Analysis

The dry potassium bromide (KBr) pellet technique was used to capture the FTIR spectra of the bacterial beads and cell pellets in triplicates after depositing a thin layer of the particles in the detector (Cary 630 FTIR). They were recorded across the range from 4000 to 500 cm^{-1} (Adzmi et al. 2012). To confirm PCC-01 association with alginate, a double-beam UV spectrophotometer (Shimadzu; Model: UV-2600) was used to measure the wavelength of the bacterial alginate beads and cell pellets between 200 and 1000 nm of triplicate samples (Tufail et al. 2022).

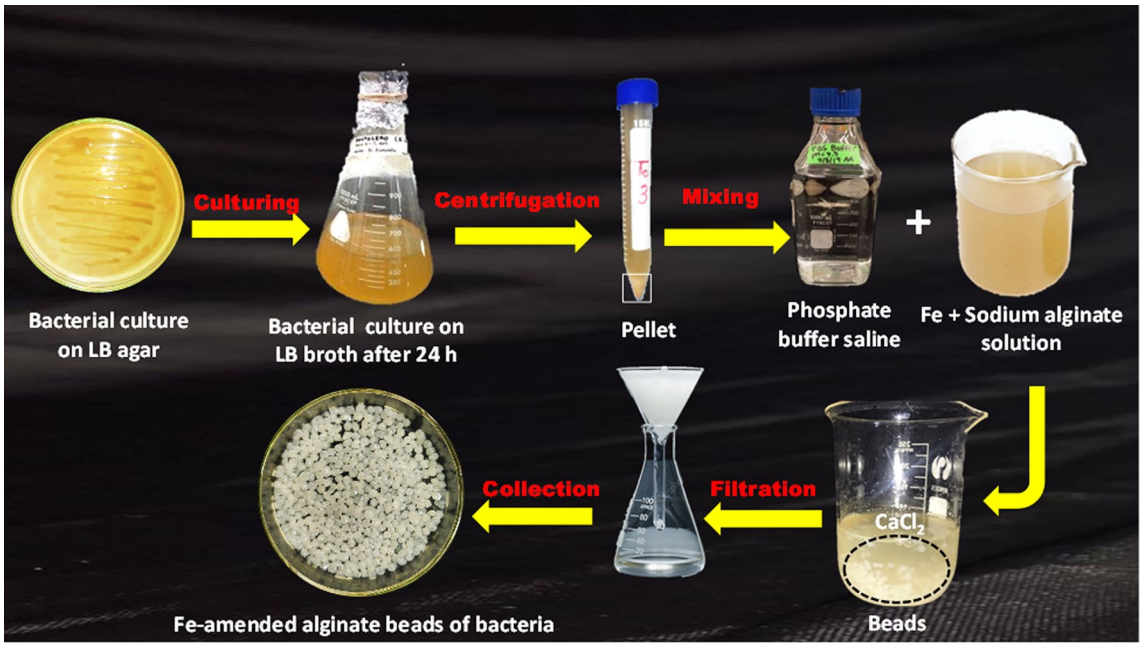

Fig. 1 Preparation of cell pellets and alginate beads of *Pseudomonas chlororaphis* subsp. *chlororaphis* (PCC-01)

Encapsulation Efficiency, Moisture Quantity, and Swelling Ratio

To measure the bacterial count in the wet capsule of beads, the beads (1 g) were mixed with saline (0.9% w/v), left for 10 min, homogenized, and finally plated on LBA (Luria–Bertani Agar) medium. After 24 h of incubation, the bacterial count of the suspension was measured by the following formula.

$$\text{Encapsulation efficiency (\%)} = \left(\frac{\text{OD of the bacterial suspension loaded in beads}}{\text{OD of the bacterial suspension}}\right) \times 100.$$

Wet beads (1 g) were dehydrated for 42 h at 30 °C (W_d) (dry weight) and the moisture content of beads (W_w) (wet weight) was measured using the following formula (Moradi-Pour et al. 2021).

$$\text{Moisture content (\%)} = \left(\frac{W_w - W_d}{W_w}\right) \times 100.$$

For the swelling ratio, about 10 mL 0.9% NaCl solution was mixed with 1 g dried beads (W_d) for 24 h. The solution was stained using the Whatman filter paper (No. 1) from the swollen bacterial beads (W_w), and the swelling ratio was calculated (Saarai et al. 2013).

$$\text{Swelling content (\%)} = \left(\frac{W_w - W_d}{W_w}\right) \times 100.$$

Particle Size

The diameters of randomly chosen wet and dried microcapsules ($n = 20$) were measured by a Vernier caliper (150 mm), and the average of 20 beads was calculated (Riaz et al. 2023).

Solubility and Slow Release of Entrapped Bacteria

The bacterial beads were vortexed after incubating in PBS (1 mL, 0.1 M) at 30 °C for 60 min. The released bacteria were recorded by measuring the absorbance of the bacterial suspension at 600 nm (Riaz et al. 2023). For slow-release test, 20 bacterial beads were placed in 75 mL sterile solution (0.85% [wt/vol] NaCl) and gently shaken for 24 h at 30 °C. Then a sample of 0.5 mL saline solution was obtained and the total number of released bacteria was quantified using the plate count method on LBA medium after incubating for 24 h at 28 °C. The whole procedure was carried out after an interval of 1, 5, 15, 30, 60, 90, and 120 days. Each treatment set was replicated three times (Riaz et al. 2023).

Greenhouse Assays Employing Agricultural Soil with PCC-01

In planta, a pot experiment was conducted to evaluate the disease-managing potential of alginate beads and cell pellets of PCC-01 in combination with Fe (Riaz et al. 2023). The experiment of seven treatments in triplicate (Table 3) was conducted in an open backfield located at 31.5204° N latitude, 74.3587° E longitude, Lahore, Pakistan for 90 days after tomato seedling transplantation during February–April, 2023 (average temperature: 25 °C ± 5 °C, average humidity: 62%). Completely random design (CRD) designed was used including experimental and control treatments (Table 3).

Prior to tomato planting, the sandy-loam garden soil (sand: 44%, silt: 30%, clay: 25%; pH: 6.80) was fumigated using a 2.5% formalin solution. For the multiplication of fungus inoculum, boiled and autoclaved millet seeds were inoculated with the fungus discs and incubated at 30 °C for 15 days. After that, fumigated soil was inoculated with colonized millet seeds (100 g/pot) containing a sclerotial count (2×10^7 sclerotia/mL), and the soil was left for 5 days. Infected soil was filled in pots (30 cm diameter × 35 cm depth) and control treatments were also prepared in a similar way but without pathogen inoculation. Five days after pathogen inoculation, the cell pellets (T_3: 0.5 g bacterial pellet; $OD_{600} = 2$) and alginate beads (T_4: 0.5 g bacterial beads; $OD_{600} = 2$) were evenly distributed and incorporated to the soil and left for another 2 days. The negative control (T_1) was treated with water, and the positive control (T_2) contained only pathogen. Finally, 3-week-old healthy tomato seedlings were transplanted to the pots (4 seedlings pot^{-1}). Tomato seedlings were prepared in a growth medium comprised of a blend of soil and peat moss in ratio 1:3 in 200-cell plastic trays (one seed per cell) using surface-sterilized seeds of Rio Grande tomato variety. The trays were kept at 21 °C ± 2.

Table 3 Treatment plan for in planta disease managing bioassays

Treatments	Description of inputs
T_1	Negative control (without pathogen/bacteria/metal)
T_2	Positive control [*M. phaseolina* (MP)]
T_3	MP + BP (0.5 g bacterial pellet; $OD_{600} = 2$)
T_4	MP + BB (0.5 g bacterial beads pot^{-1}, $OD_{600} = 2$)
T_5	MP + Fe (0.0005% pot^{-1})
T_6	MP + Fe-amended BP (Fe-BP: 0.5 g bacterial pellets pot^{-1}, $OD_{600} = 2$)
T_7	MP + Fe-amended BB (Fe-BB: 0.5 g bacterial beads pot^{-1}, $OD_{600} = 2$)

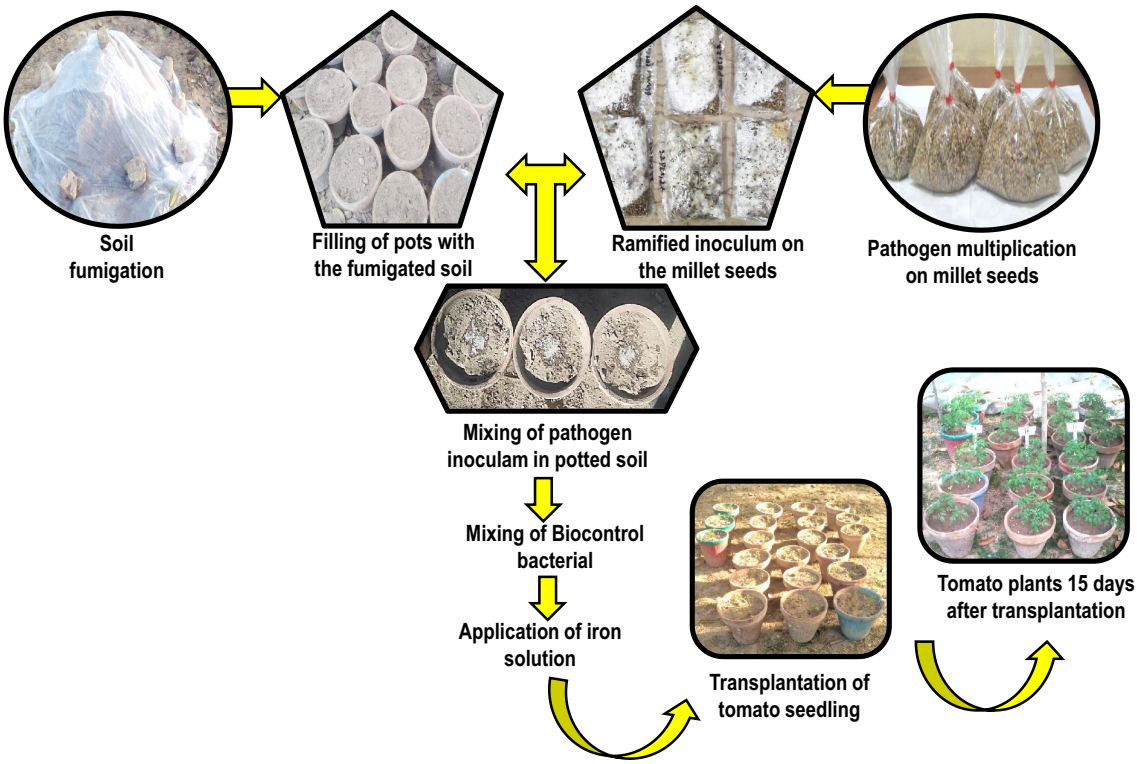

Fig. 2 Experimental steps for in planta assays

Rio Grande tomato variety was chosen for their broad geographic adaptability and strong agronomic/horticultural performance (Fig. 2).

Disease Measurements

The disease severity caused by *M. phaseolina* in tomato plants was visibly assessed on the 90th day post-seedling transplant. Each plant was evaluated and graded from 0 to 5 based on the symptoms (Table 4) and the percentage of disease severity index (DSI) was calculated using the equation described by Shoaib et al. (2021).

$$\text{DSI (\%)} = \sum \left(\frac{\text{Severity rating} \times \text{Number of plants in the rating}}{\text{Total number of plants used in the rating} \times \text{Maximal DS score}} \right) \times 100.$$

Vegetative and Reproductive Indices

Ninety days after transplanting, the plants were carefully separated from the soil and rinsed with tap water.

Table 4 A disease rating scale for ranking of charcoal rot disease severity

Grade	Disease severity	Status	Symptoms
0	0%	Highly resistant	No pathogen attack
1	1–9%	Resistant	Plants resist infection and have no external symptoms (stem and root blackening, leaf chlorosis, reduction of fruit size and number)
2	10–24%	Moderately resistant	Minor symptoms
3	25–49%	Moderately susceptible	Moderate symptoms
4	50–74%	Susceptible	Severe symptoms
5	75% and above	Highly susceptible	The whole plant become wilt and severe infection occurs

Following harvest, plant height, fresh shoot and dry shoot weight, fresh root weight and dry root weight, root length, and shoot length were measured for the triplicate samples of each treatment ($n = 3$). Tomatoes were harvested manually once they reached commercial maturity (fully red color). Reproductive indices like the number, weight, and size of tomatoes were recorded. The ripe tomato fruits were harvested every 3 days during the period from 75 days until 90 days post-transplantation.

Economic Analysis

Tomato fruits were graded based on their number, mass, and diameter (Table 5). The undamaged fruits were classified as marketable. The harvest index was determined as a ratio between marketable fruits and total plant biomass and was expressed as a percentage (Awan et al. 2023).

$$\text{Harvest Index } (\%) = \left(\frac{\text{Tomato yield}}{\text{Biological yield}}\right) \times 100.$$

Biochemical Assays

Three leaf samples from each replicate of each treatment on day 40th after seedling transplanting were collected for biochemical assays. Total chlorophyll content (TCC) and carotenoids (CC) were determined by homogenizing 0.5 g plant leaves in 80% ethanol. The resulting material was centrifuged at 10,000 rpm for 10 min, and the absorbance of the supernatant was measured for chlorophyll A (645 nm), chlorophyll B (663 nm), and carotenoids (470 nm) against a blank. For total protein content (TPC), leaf extracts (0.5 g leaf samples in 10 mL sodium phosphate buffer, pH 7.5) were centrifuged for 10 min at 3000 rpm. The supernatant (0.1 mL) was diluted to 1 mL and mixed with Reagent C, containing copper sulfate (0.5%), sodium carbonate (50 mL at 2 g), sodium hydroxide (0.4 g at 0.1 mol L^{-1}), and sodium potassium tartrate (1 g in 100 mL distilled water). After adding 0.1 mL 50% Folin–Ciocalteu reagent, samples were incubated at room temperature for 30 min. Absorbance was measured at 650 nm, with various concentrations of bovine serum albumin (BSA) used as standards. Catalase (CAT, EC: 1.11.1.6) activity was measured using 0.1 mL enzyme extract and 2.9 mL 0.106 mol L^{-1} H_2O_2 in 50 mmol L^{-1} potassium phosphate buffer at 240 nm. For peroxidase (POX, EC 1.11.1.7), a mixture of 0.5 mL enzyme extract, 2 mL 0.1 mol L^{-1} phosphate buffer, 1 mL pyrogallol, and 1 mL 0.05 mol L^{-1} H_2O_2 was incubated at 25 °C. Total purpurogallin was calculated by adding 2.5 mol L^{-1} H_2SO_4, and absorbance was measured at 420 nm. Phenylalanine ammonia-lyase (PAL: EC 4.3.1.5) activity was determined at 290 nm by analyzing trans-cinnamic acid production with 0.4 mL enzyme extract, 1.1 mL 0.1 mol L^{-1} sodium borate buffer (pH 8.8), and 0.5 mL 0.012 mmol L^{-1} L-phenylalanine. Polyphenol oxidase (PPO, EC 1.14.18.1) activity was determined by using 0.2 mL enzyme extract, 1.5 mL sodium phosphate buffer (0.1 mol L^{-1}; pH 6.5), and 0.2 mL freshly prepared catechol (0.01 mol L^{-1}). Absorbance of the reaction mixture for PPO activity was measured at 495 nm at 30 s intervals for 3 min against a blank (Nafisa et al. 2020; Shoaib et al. 2021; Yaqoob et al. 2024).

Table 5 Grading basis of tomato fruits

Fruit number	Mass (g)	Diameter ($mm^{2)}$	Grading
8–10	24–32	30–35	A
5–7	13–24	25–30	B
1–4	0–12	20–25	C

Histo-chemical Studies

Five to six free-hand stem sections (5–10 µm) after 40 days of transplantation were processed for histo-chemical investigation. Wiesner's staining was employed to detect lignin accumulation. A solution was prepared by mixing 3% (w/v) phloroglucinol in 100% ethanol with HCl (37 N) in a ratio of 2:1 to create the freshly prepared Wiesner's reagent (phloroglucinol-HCl). The stem sections were treated with this reagent, and after 30–60 s, they were observed under a bright-field microscope (Nizam et al. 2023). For the phenol accumulation using ferric chloride test, stem sections were submerged in a 10% ferric chloride solution, staining them for 30 min. Following this, the sections were thoroughly washed with distilled water to remove any excess stain (Riaz et al. 2023). For starch detection, through an iodine-potassium solution, the sections underwent a thorough washing with autoclaved distilled water following immersion in 2% iodine-potassium solution for 5 min (Schaker et al. 2017). After dyeing by using the different reagents, the stem cuttings were examined under the light microscope for lignin, phenolic, and starch deposition.

Statistical Analysis

The statistical design was a completely randomized, and the means were compared based on the LSD (least significance difference) test with an alpha error level of 5% using the software Statiatix 8.1. Differences were significant at the 0.05% level. Heat maps, principal components, and hierarchical clustering analysis were developed to summarize the variability of the treatment and identify the relation between the observed attributes across the all experiments.

Results

Pathogenicity Assays

The pathogenicity test revealed that *M. phaseolina* was highly virulent on *S. lycopersicum* fruit. The relative infected area (%) increased significantly on the 7th day after inoculation (DAI), while fruits appeared soft and decayed. There was 100% infection on the 20th DAI. No symptoms were found in the control. After the pathogenicity trial, macroscopic confirmation of the fungus was carried out and the observed growth pattern of the colony (blackish gray with dense mycelial growth), hyphae (brown and septate), and sclerotia (brownish-black and round to ovoid) confirmedthat the isolated fungus was the same as the one inoculated on the tomato fruit (Fig. 3).

Screening of Potential Bacterial Strain Against *M. phaseolina*

All four bacterial strains, i.e., *B. amyloliquefaciens* (BA-01), *P. chlororaphis* subsp. *chlororaphis* (PCC-01), *P. chlororaphis* subsp. *aurantiara* (PCA-02), and *P. aurantiara* (PA-03) had significantly ($p < 0.05$) greater antifungal activity against *M. phaseolina* compared to the control. Three of the bacterial strains, viz., BA-01, PCA-02, and PA-03, exhibited ~60% inhibition in fungal growth. PCC-01 exhibited the maximum inhibition of 71% in the fungal growth; therefore, this bacterial strain was characterized as a very strong antagonist and was used for further experiments (Fig. 4).

Evaluation of PCC-01 for Plant Growth-Promoting Traits

Phosphate solubilization potential of PCC-01 was observed with the appearance of colorless halos surrounding the colony, indicating that this test was positive in the potential bacterial strain (Fig. 5A). PCC-01 was able to produce HCN as transformations from yellow to radish color were noticed (Fig. 5B). The existence of IAA was confirmed by measuring pink coloration as compared to the control (Fig. 5C). The change in color from green to deep pink with 0.0005% aqueous $FeSO_4$ confirmed the Fe solubilization by PCC-01 (Fig. 5D).

Characterization of Alginate Beads of PCC-01

FTIR

FTIR of alginate beads was compared with cell pellets for the confirmation of the association of the PCC-01 within alginate beads. Major peaks [3372, 3317, 3302 cm^{-1}

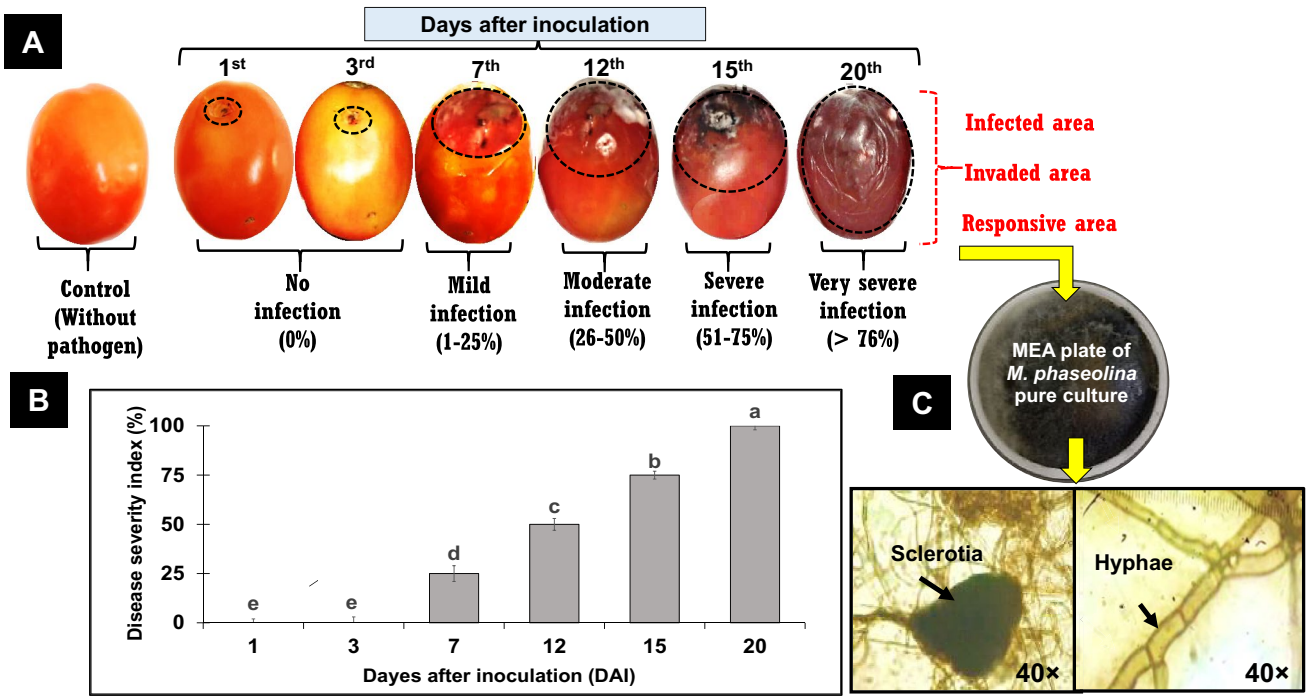

Fig. 3 **A**–**C** Pathogenicity test of *Macrophomina phaseolina* on *Solanum lycopersicum* fruit. **A** Infection formed on fruit as compared to control; **B** the vertical bar shows standard error ($n = 4$), and the alphabets show a significant difference (LSD test, $p \leq 0.05$); **C** isolation and identification of the pathogen from the infected tomato fruit

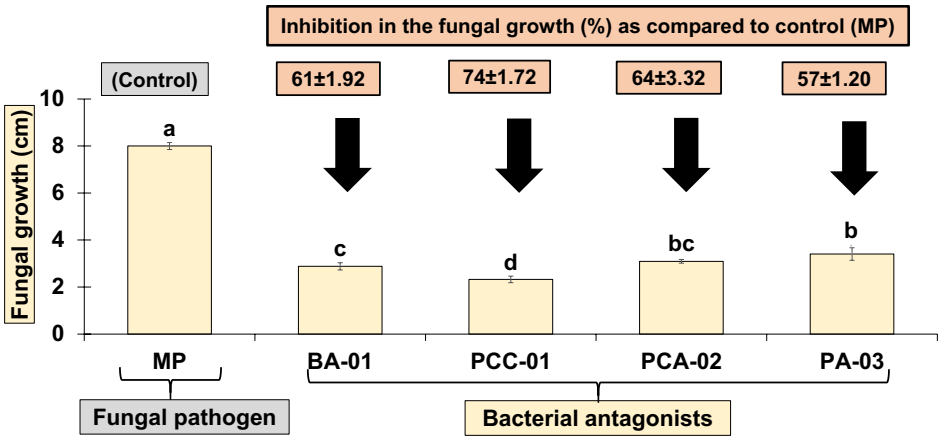

Fig. 4 Antagonistic effect of bacterial strains against *Macrophomina phaseolina* by dual culture assays on 2% malt extract agar plates 7 days after incubation at 30 °C. MP: *Macrophomina phaseolina*; BA-01: *Bacillus amyloliquefaciens*; PCC-01: *Pseudomonas chlororaphis* subsp. *chlororaphis*; PCA-02: *Pseudomonas chlororaphis* subsp. *aurantiaca*; PA-03: *Pseudomonas aurantiaca.* In the Petri plates, the letters L (longest) and W (horizontal) represent the diameter of the fungus growth. The vertical bar shows standard error ($n = 4$), and the alphabets show a significant difference (LSD test, $p \leq 0.05$)

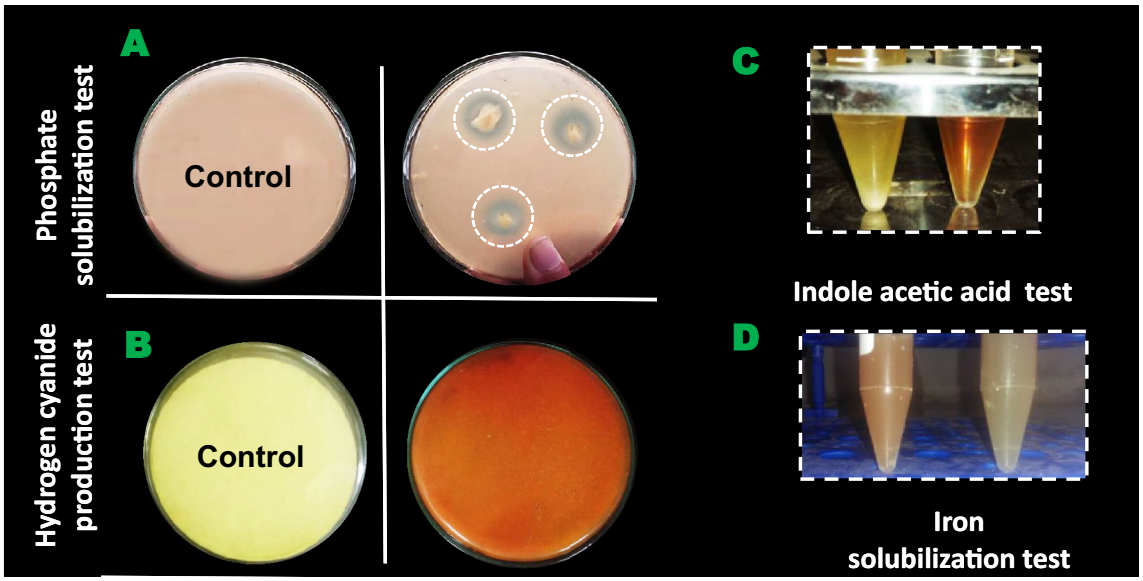

Fig. 5 In vitro antifungal and plant growth-promoting traits of *Pseudomonas chlororaphis* subsp. *chlororaphis* (PCC-01). **A** Colorless halos showing phosphate solubilizing activity; **B** development of pink color specified HCN production; **C** pink coloration indicating IAA production; **D** pink color with aqueous $FeSO_4$ confirmed the Fe solubilization

(carbohydrate), 1596 cm^{-1} (nucleic acid), 1421, 1416 cm^{-1} (protein), 1326 cm^{-1} (lipid), 1297 cm^{-1} (amide-III), and 1027 cm^{-1} (nucleic acid)] revealed the occurrence of the primary constituents of the cell (lipids, proteins, and nucleic acids) in the cell pellet. The spectra of bacterial alginate beads have similarities with those of bacterial cell pellets, though intensity variation between the spectra observed particularly at protein regions (highlighted) indicated PCC-01 and alginate have a good affinity, thus establishing chemical interactions (Table 6; Fig. 6).

UV Absorption Spectra

The UV–VIS–IR (190 nm/1100 nm) radiation absorbance profiling of PCC-01 cell pellet and alginate beads revealed an absorbance range between 200 and 900 nm. The profiles generated using pellet and alginate beads demonstrated the

Table 6 FTIR wave number assignment to function groups

Cell pellet	Alginate beads	Functional groups
3372, 3317, 3302	3309, 3280	$-NH_2$ of amines and –OH groups proteins and carbohydrates
2594, 2571	2594, 2556	(–SH stretching)
1632	1640	(COO–), proteins
1596	–	NH_2 or (C–N), Nucleic acids
1679	–	(Amide I band, β-sheet), Protein secondary structure
1421, 1416	–	C=O stretching (amide I band), protein secondary structure
1401	–	(CH, CH_3), proteins
1326	1304	Lipids
1297	-	(Amide III band), proteins
1252		(Amide I band), protein secondary structure
1162, 1148	–	(C–O) glucose and fructose, Carbohydrates
1027	–	C–O, ribose, nucleic acids

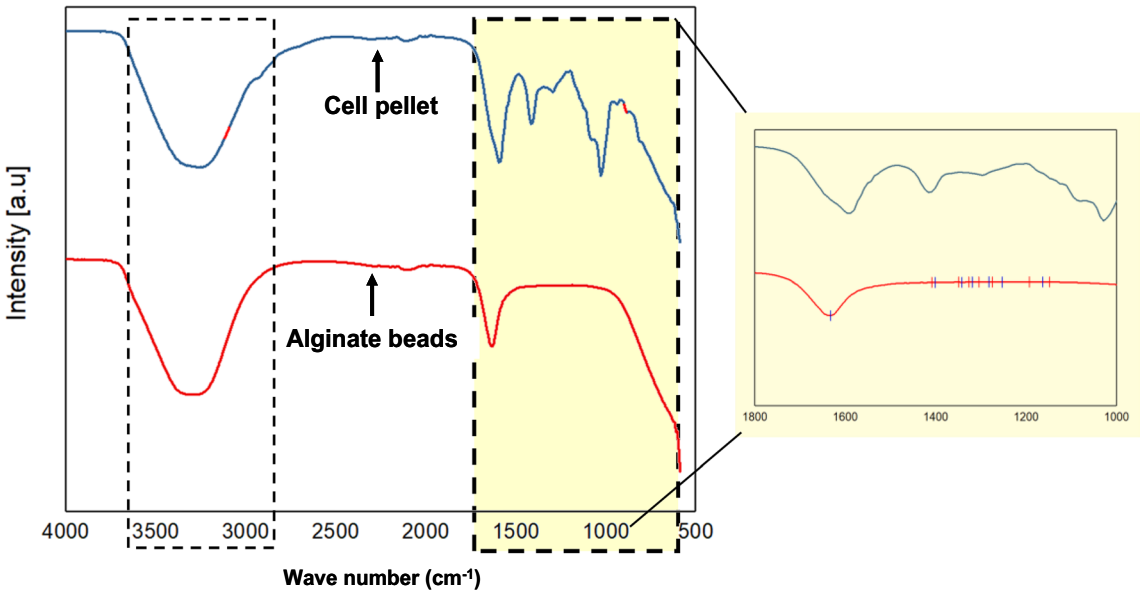

Fig. 6 Fourier Transform Infrared (FTIR) spectra of cell pellet and alginate beads of *Pseudomonas chlororaphis* subsp. *chlororaphis* (PCC-01)

same highest absorbance peak at ≅235 nm without peak dislocation, as well as no significant alteration in the absorbance pattern (Fig. 7).

Encapsulation Efficiency, Moisture Content, Swelling Ratio, Size, and Solubility

The bacterial alginate beads exhibited encapsulation efficiency, moisture content, and swelling ratio of 93.14, 92.15, and 66.47%, respectively, along with wet and dry particle sizes of 3.31 mm and 2.70 mm, respectively. The solubility test of entrapped bacteria revealed the release considerable bacteria (OD_{600} = 2.26) from the alginate beads (Table 7).

Viability Test

It is critical for the beads to retain bacteria to predict their long-term availability in soil. The release rate of bacteria from the bead remained the same (OD_{600} = 2.01) statistically till the 30th day and decrease significantly by 18, 40, and 87% after 60, 90, and 120 days, respectively (Fig. 8).

In Planta Bioassays

Disease Severity and Disease Incidence

The disease symptoms on *M. phaseolina* (MP) in inoculated plants, recorded as stem blackening and leaf chlorosis, along

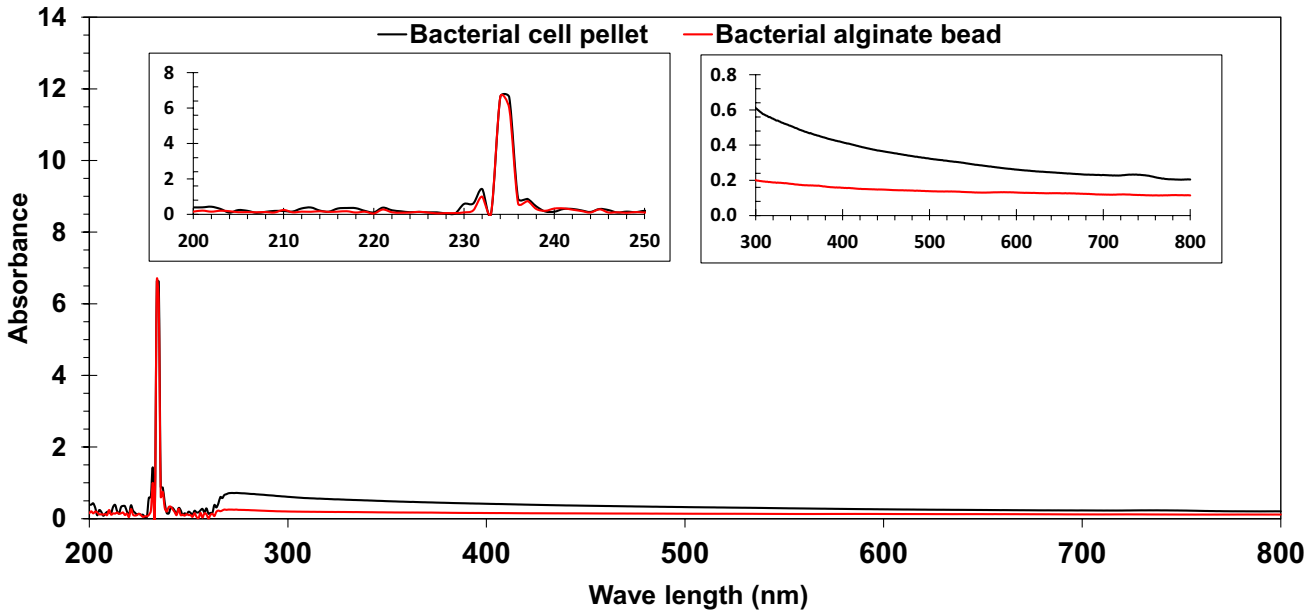

Fig. 7 UV spectra of cell pellet and alginate beads of *Pseudomonas chlororaphis* subsp. *chlororaphis* (PCC-01)

Table 7 Characterization of alginate beads of *Pseudomonas chlororaphis* subsp. *chlororaphis* (PCC-01)

Characteristics	Value
Encapsulation efficiency (%)	96.20 ± 1.01
Moisture content (%)	92.50 ± 0.82
Swelling ratio (%)	66.47 ± 0.91
Wet particle size (mm)	3.30 ± 2.38
Dry particle size (mm)	2.70 ± 2.10
Wet particle weight (mg)	15.01 ± 3.71
Dry particle weight (mg)	0.70 ± 0.23
Release of bacteria (OD_{600}) after solubility in PBS	2.26 ± 1.60

± indicates the mean of triplicate

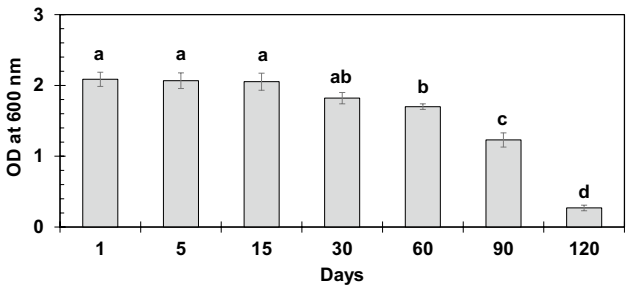

Fig. 8 Slow release of bacteria from the alginate beads of *Pseudomonas chlororaphis* subsp. *chlororaphis* (PCC-01). Data in triplicate ($n = 3$) are shown as error bars, while alphabets on the bar graph show a significant difference ($p \leq 0.05$) as determined by the LSD test

with reduction in leaf area, fruit size, and fruit quantity, were detected (T_2: positive control) at 90 days post-transplantation by the end of April. Thus in T_2, there was the maximum disease severity index (DSI: 75%) and disease incidence (DI: 100%) (Figs. 9 and 10). Other treatments significantly decreased disease; hence, the application of PCC-01 either as pellets (T_3: BP) or beads (T_4: BB) exhibited fewer symptoms and showed statistically the same DSI: ~25% and DI: ~35%, and the plants in these treatments were ranked under moderately resistant group. The application of Fe (T_5) showed ~50% DSI and DI due to which the plants were kept under moderately susceptible group. However, there was significantly lower disease incidence in Fe-BP (T_6: DSI and DI: 12%) and Fe-BB (T_7: DSI and DI: 4%), categorizing the plants as moderately resistant and resistant, respectively, against the fungal infection (Figs. 9 and 10).

Vegetative Indices

The plants in the positive control (T_2, without MP or PCC-01) exhibited a 30–60% reduction in length and biomass as compared to the negative control (T_1). T_2 exhibited the lowest lengths, fresh biomass, and dry biomass of shoot and root, respectively. All other treatments (T_3–T_7) significantly and variably improved shoot length, fresh and dry biomass by 30–40%, 300–500%, and 100–200%, respectively, and the same attributes of the root by 30–70%, 200–240%, and 100–200%, respectively, as compared to T_2. For most of the growth indices, bacterial beads + Fe (T_7) followed by

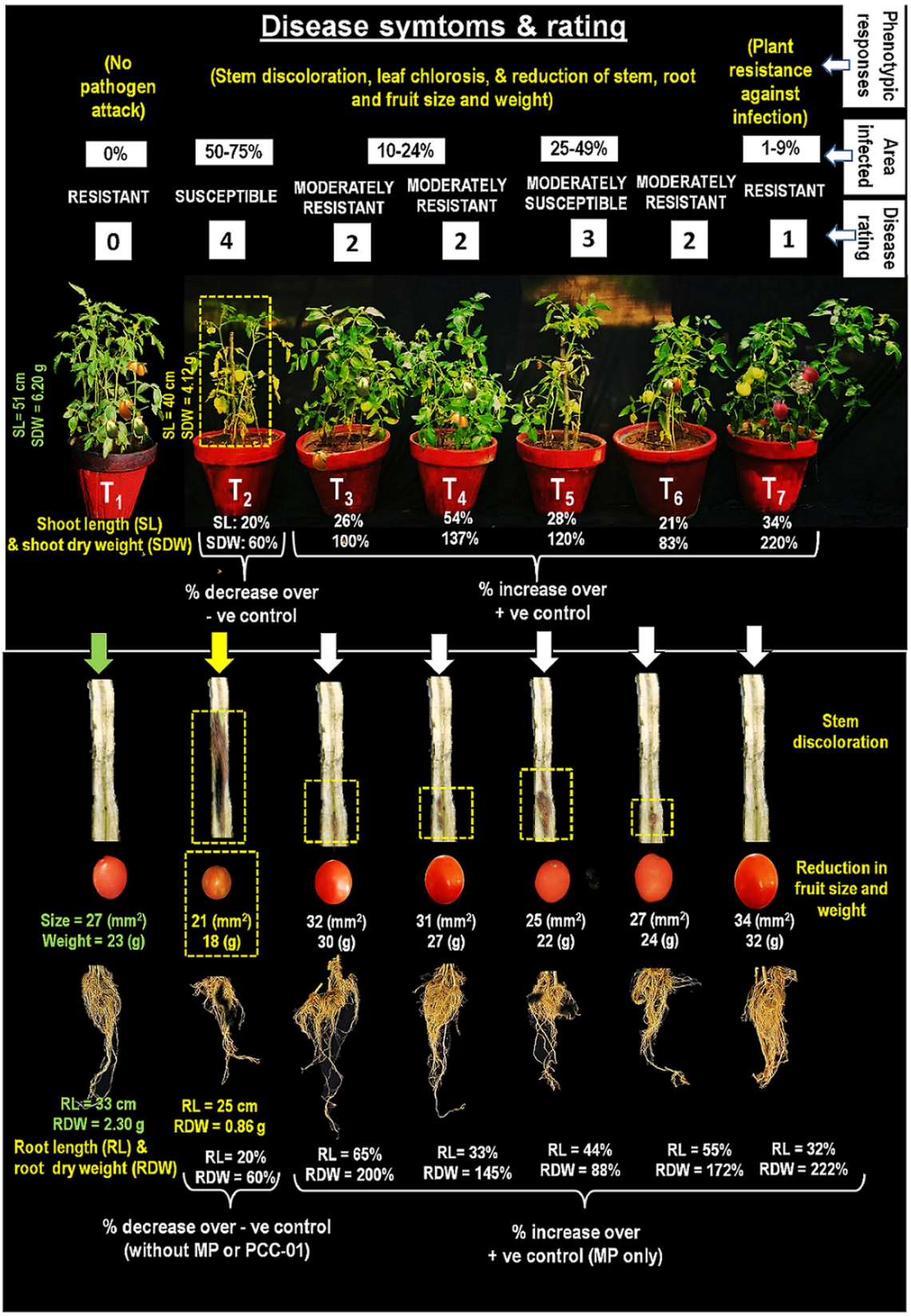

Fig. 9 Effect of *Pseudomonas chlororaphis* subsp. *chlororaphis* (PCC-01) and iron (Fe) on the disease and growth of *Solanum lycopersicum* plants under *Macrophomina phaseolina* (MP) stress. T_1: (−ve control); T_2: (+ve control); T_3: (MP + BP); T_4: (MP + BB); T_5: (MP + Fe); T_6: (MP + Fe-BP); and T_7: (MP + Fe-BB). BP and BB stand for bacterial pellet and bacterial beads, respectively

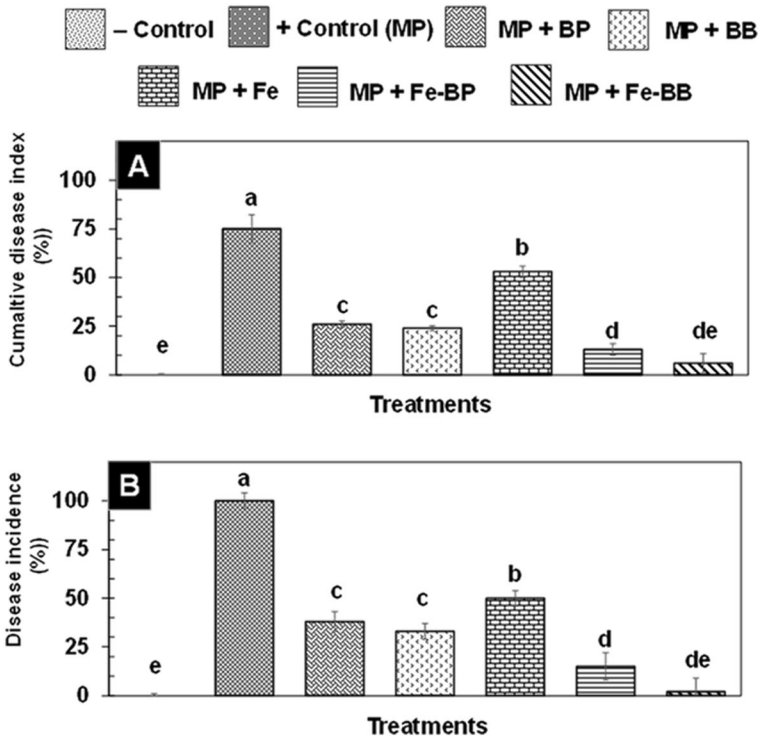

Fig. 10 **A**, **B** Effect of iron (Fe)-supplemented alginate beads of *Pseudomonas chlororaphis* subsp. *chlororaphis* (PCC-01) on the cumulative disease index (**A**) and disease incidence (**B**) in *Solanum lycopersicum* plants caused by *Macrophomina phaseolina* (MP). BP and BB are bacterial pellet and bacterial beads, respectively. Error bars on the bars indicate the mean of replicates ($n = 3$) and different letters denote significant differences according to the LSD test ($p \leq 0.05$)

bacterial pellets + Fe (T_6) exhibited similar or greater growth indices compared to T_1 (Fig. 11).

Reproductive Indices

Reproductive attributes including fruit number, weight, diameter, and length were significantly reduced by 20–30% in T_2 as compared to T_1. The mean number, weight, diameter, and length of fruits in T_7 was significantly larger by 20% and 100% than that of T_1 and T_2, respectively. T_4, followed by T_3, and T_6 also exhibited 50–80%, 40–60%, and 20–50% higher attributes of yield as compared to T_2. T_3, T_4, and T_6 exhibited 20–30% greater attributes than T_1 as well, though these were insignificantly different from each other and with T_1 in many cases. There was no difference between the fruit number and weight of T_2 and T_5, whereas T_5 treatment showed a significant increase in fruit diameter and length by 20–30% as compared to T_2 (Fig. 12).

On the basis of number, mass, and diameter, tomato fruits were categorized as A, B, and C. Data indicated that plants in T_1 produced the highest number of "B" grade tomatoes (65%) followed by the equal number of "A" and "C" grades. However, the number of "C" grade tomatoes was maximum (60%) followed by "B" (40%) in T_2. The rest of the treatments displayed better quality of tomatoes. T_7 produced the highest "A" (65%) and the lowest "B" (25%) grade tomatoes, and the lowest "C" (10%) grade tomatoes. The second-best treatment was T_4 giving 50% "A," 35% "B," and 15% "C" grade tomatoes. This was closely followed by T_3 and T_6. Fe alone in T_5 showed 20% "A," 45% "B," and 35% "C" grade tomatoes (Table 8).

Economic Analysis

The biological yield (BY plant^{-1}), tomato yield (TY plant^{-1}), and harvest index (HI) of 21.25 g, 12.77 g, and 60.08%, respectively, were recorded with T_1. All other treatments (T_3–T_7) significantly managed charcoal rot disease in tomato plants by giving greater values of BY, TY, and HI as compared to obtained with T_2. However, the maximum HI of 63.50% was obtained with MP + Fe-BB, followed by 61.80% with T_3 and T_4 and 57.50% with T_5 and T_6, respectively (Table 9).

Physico-biochemical Assays

Plants subjected to *M. phaseolina* showed stress and significantly 32% reduction in leaf total chlorophyll content and carotenoids (T_2: positive control) contrasted to the negative control. The photosynthetic pigments have been improved significantly by 30–50% in the remaining treatments as compared to T_2 (Fig. 13A, B).

The activity of POX was not affected significantly in T_2 as contrast to T_1, even though the production of PPO and PAL dropped significantly by 60% over T_1. In the rest of the treatments, the expression of POX, PPO, and PAL enhanced significantly by 23–55%, 185–287%, and

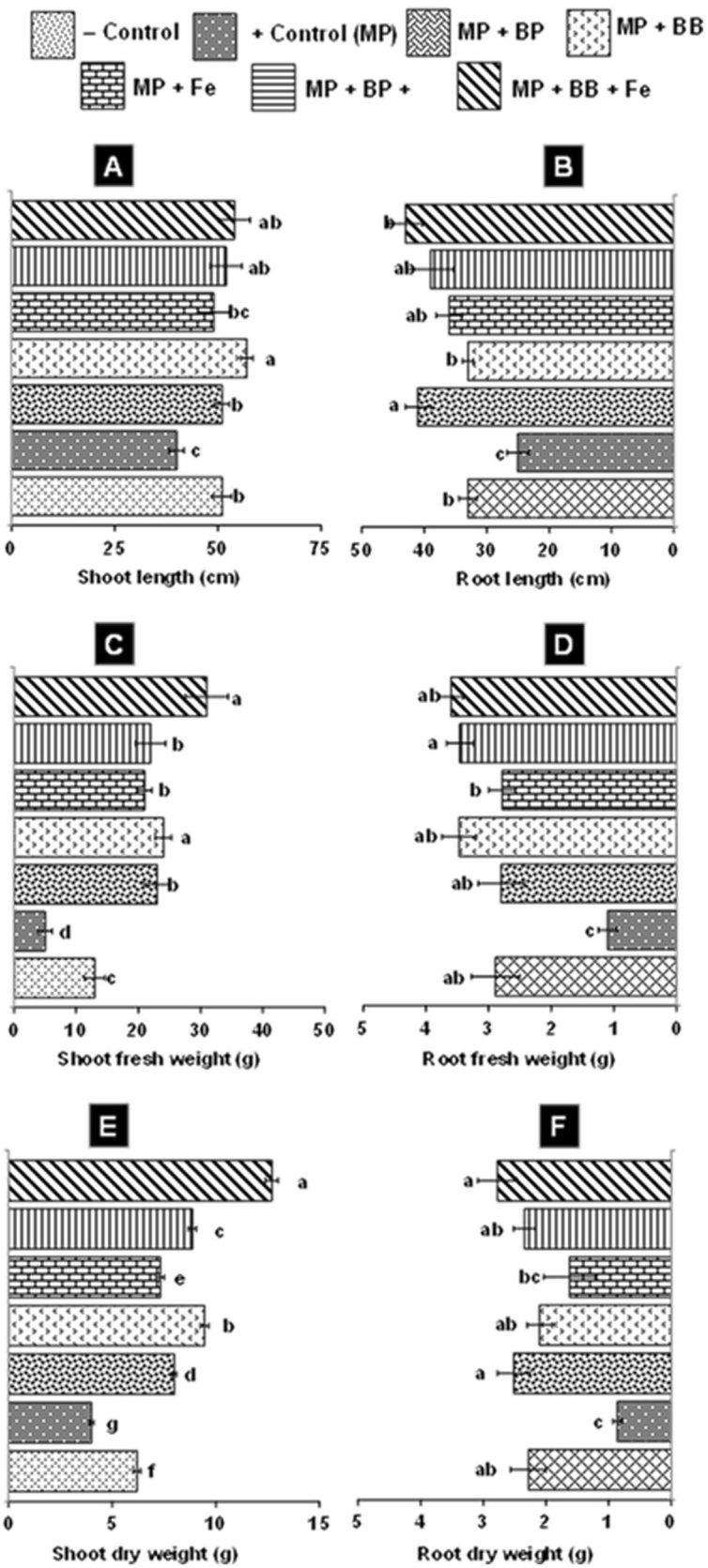

Fig. 11 **A**–**F** Effect of iron (Fe)-supplemented alginate beads on growth and biomass of 90-day-old *Solanum lycopersicum* plants under *Macrophomina phaseolina* (MP) stress. BP and BB are bacterial pellet and bacterial beads, respectively. Error bars on the bars indicate the mean of replicates ($n = 3$) and different letters denote significant differences according to the LSD test ($p \leq 0.05$)

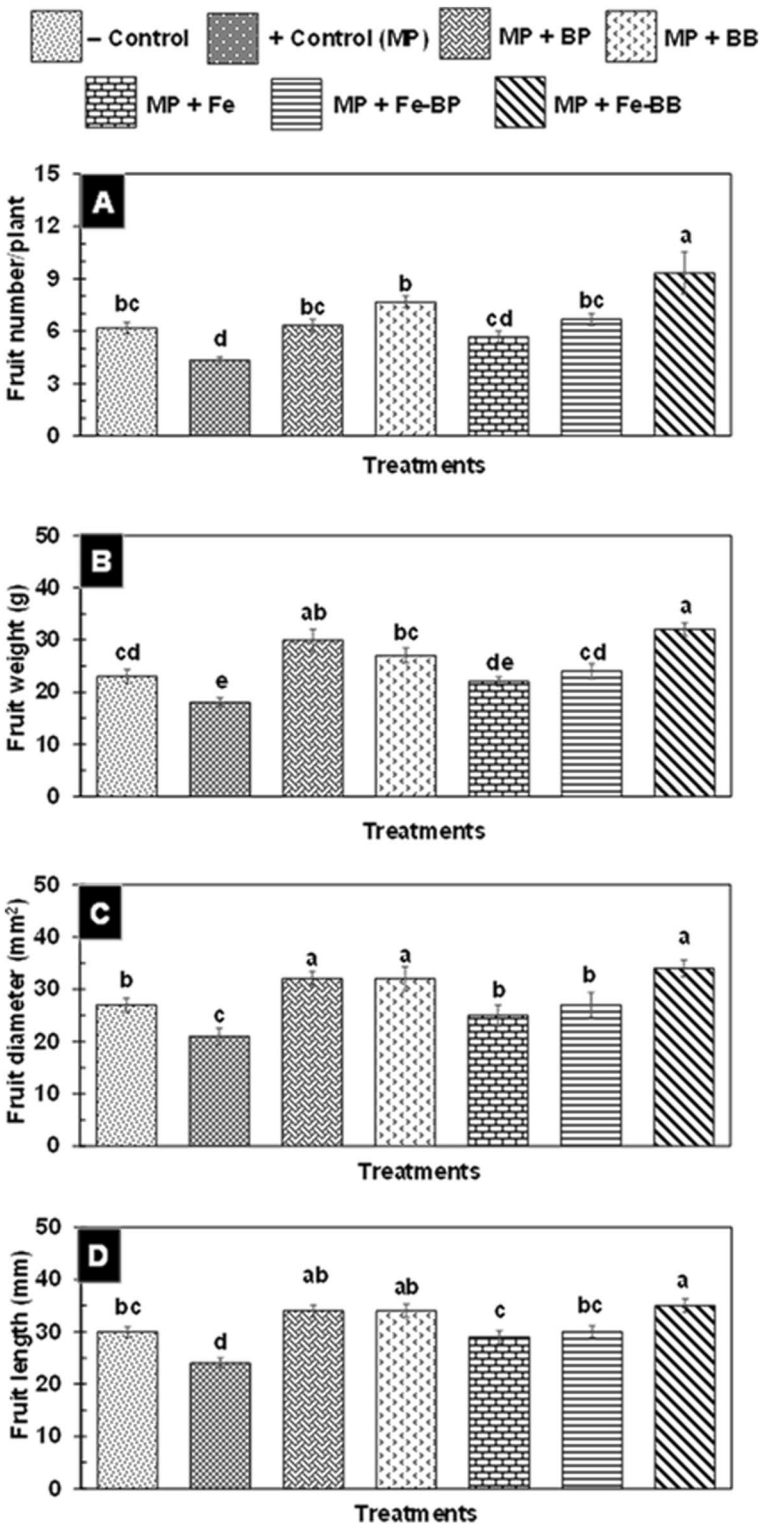

Fig. 12 **A**–**D** Effect of iron (Fe)-supplemented alginate beads of *Pseudomonas chlororaphis* subsp. *chlororaphis* (PCC-01) on yield attributes of 90-day-old *Solanum lycopersicum* plants under *Macrophomina phaseolina* (MP) stress. BP and BB are bacterial pellet and bacterial beads, respectively. Error bars on the bars indicate the mean of replicates ($n = 3$) and different letters denote significant differences according to the LSD test ($p \leq 0.05$)

198–260%, respectively, in comparison to T_2. The maximum increase was recorded in T_7, followed by T_6, T_5, T_4, and T_3 (Fig. 13C–E).

Histo-chemical Assays

Phloroglucinol reacted with cinnamaldehyde end-groups of lignin to yield either pink pigments (hydroxycinnamic

Table 8 Effect of *Pseudomonas chlororaphis* subsp. *chlororaphis* (PCC-01) and iron (Fe) on the quality of tomato under the stress of *Macrophomina phaseolina* (MP)

Treatments		Grading percentage of tomato		
		A	B	C
T_1	−ve control	4	13	3
T_2	+ve control (MP only)	0	8	12
T_3	MP + BP	9	7	4
T_4	MP + BB	10	7	3
T_5	MP + Fe	4	9	7
T_6	MP + Fe-BP	8	8	4
T_7	MP + Fe-BB	13	5	2

BP and BB stand for bacterial pellet and bacterial beads, respectively

Table 9 Economic analysis of tomatoes due to effect of *Pseudomonas chlororaphis* subsp. *chlororaphis* (PCC-01) and iron (Fe) under *Macrophomina phaseolina* (MP) stress

Treatments	Biological yield (g plant^{-1})	Tomato yield (g plant^{-1})	Harvest index (%)
−ve control	21.25	12.77	60.08
+ve control (MP)	9.56	4.70	49.15
MP + BP	27.61	17.10	61.93
MP + BB	30.18	18.63	61.73
MP + Fe	20.16	11.23	55.70
MP + Fe-BP	25.61	14.41	56.26
MP + Fe-BB	42.35	26.88	63.47

BP and BB stand for bacterial pellet and bacterial beads, respectively

aldehydes) or red-brown pigments (hydroxybenzaldehydes). The intensity of color made it much easier to observe the level of lignification in different treatments in a qualitative manner. The vessels and interfascicular fibers of the xylem were the only elements of the stem that were stained by the lignin stains (phloroglucinol). In T_1, the stem section showed brighter red coloration suggesting a higher level of hydroxybenzaldehydes, while lignin degraded in the tissues of positive control (T_2) as indicated by the change in the color intensity. In the rest of the treatments, the xylem was stained in different shades of pink-violet specified enrichment of hydroxycinnamic aldehydes due to enhanced resistance against the pathogen.

The ferric chloride test is based on the reaction of tannic acid with mucilages and pectin substances, to produce a gray-black color. Staining with ferric chloride clearly showed phenolic deposition in stem sections of all seven treatments. The contact of the plants with the pathogen in T_2 resulted in substantial damage to the epidermis, cortex, and pith region and less accumulation of phenolic compared with T_1. These regions were intact in the rest of the treatments in T_3–T_7, and there was more deposition of phenolic (Fig. 14).

An iodine test detects the presence of starch in the form of granules; depending on the proportion of amylose in the starch, the reaction between iodine and amylose forms a poly-iodide chain that is typically deep blue or brown-black. The analysis revealed starch granules stained in violet-black color in the negative control. By comparison, the lowest starch accumulation was observed along with yellow coloration of the vascular region, epidermis, cortical region, and pith due to the degradation of deposited starch granules by starch-hydrolytic enzymes of the *M. phaseolina* in the positive control. The remaining treatments clearly showed the presence of starch grains, whereas, in T_3, T_5, and T_7, these were noticed in abundance (Fig. 14).

Multivariate Analysis

PCA-based biplot, cluster analysis, and heat map were performed to identify potential treatments against the disease in tomato plants in response to *M. phaseolina*, biocontrol bacteria, and essential metal (Fe). PCA analyses with all 15 traits including disease, growth parameters, yield, and biochemical-related indices of tomato plants displayed a fine separation between treatments, both in treated and non-treated conditions (Fig. 15A, B). The first two principal components (PCs) accounted for 86.49% of the total variation among all 7 treatments that were separated into four groups. In group I, the negative control (T_1) was at the lower right side, while in group VI, the positive control (T_2) was at the lower left side of the biplot due to the occurrence of charcoal rot disease in T_2. The locations of the treatments, viz., T_7 followed by T_6, T_4, and T_3 in group II and T_5 in group III on the upper-right side of the biplot, exhibited greater attributes of morph growth, yield, biochemical, and gene expression with the minimum occurrence of charcoal rot disease in the tomato plants as compared to T_2 (Fig. 15A). PCA was performed to explicate all hidden correlations between all the treatments and to extract linear combinations of strongly correlated variables. All growth parameters on the right side indicated their positive relation to each other and negative association with the disease (Fig. 15B). The cluster dendrogram (Fig. 15C) shows the average linkage method of hierarchical clustering of all treatments (T_1–T_7).

Differences between the treatments were evaluated by visualizing the heat map and contributed greater importance to the separation of treatments into different categories. Treatments showing the highest values for the measured morpho-physiological parameters, located in the upper-right corner of the heat map, were considered highly resistant to the attack of *M. phaseolina* and had greater growth, yield,

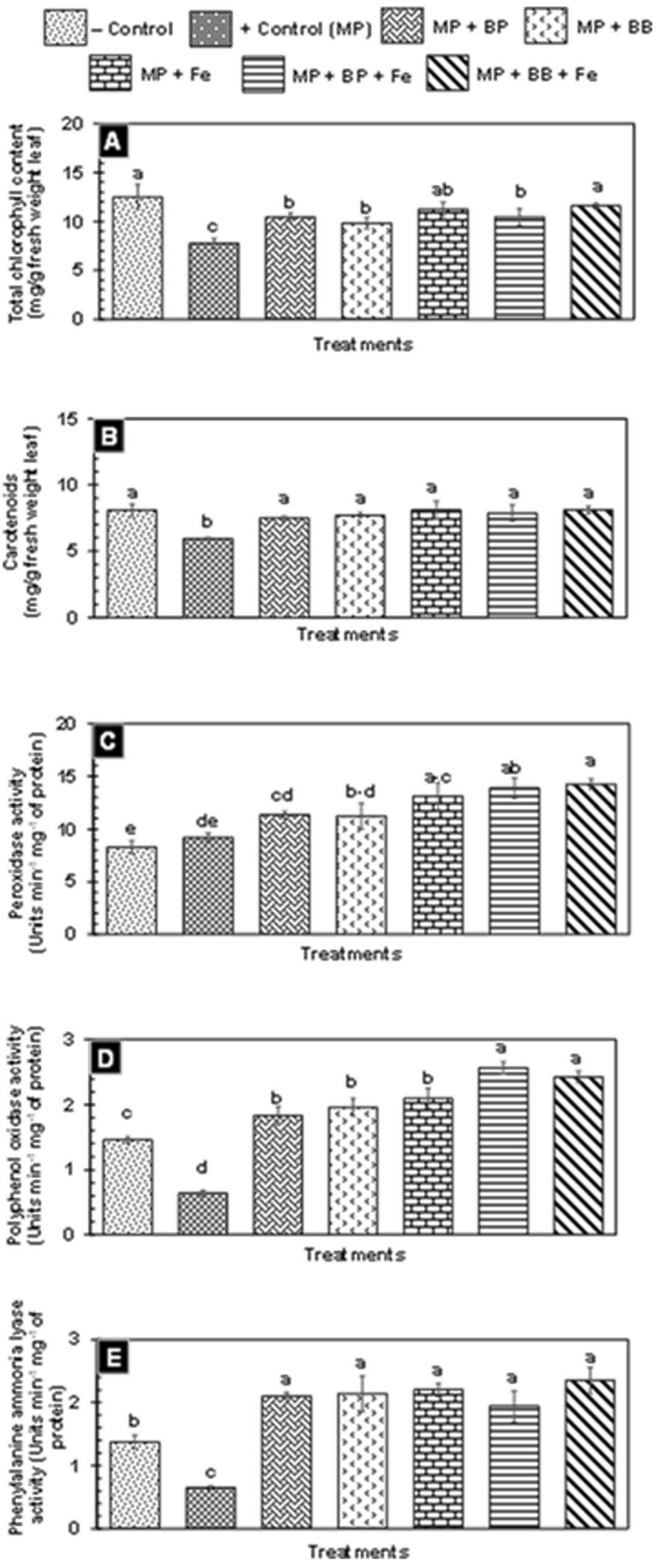

Fig. 13 Effect of Fe-supplemented alginate beads of *Pseudomonas chlororaphis* subsp. *chlororaphis* (PCC-01) on physicochemical attributes of 40-day-old *Solanum lycopersicum* plants under *Macrophomina phaseolina* (MP) stress. BP and BB are bacterial pellet and bacterial beads, respectively. Error bars on the bars indicate the mean of replicates ($n = 3$) and different letters denote significant differences according to the LSD test ($p \leq 0.05$)

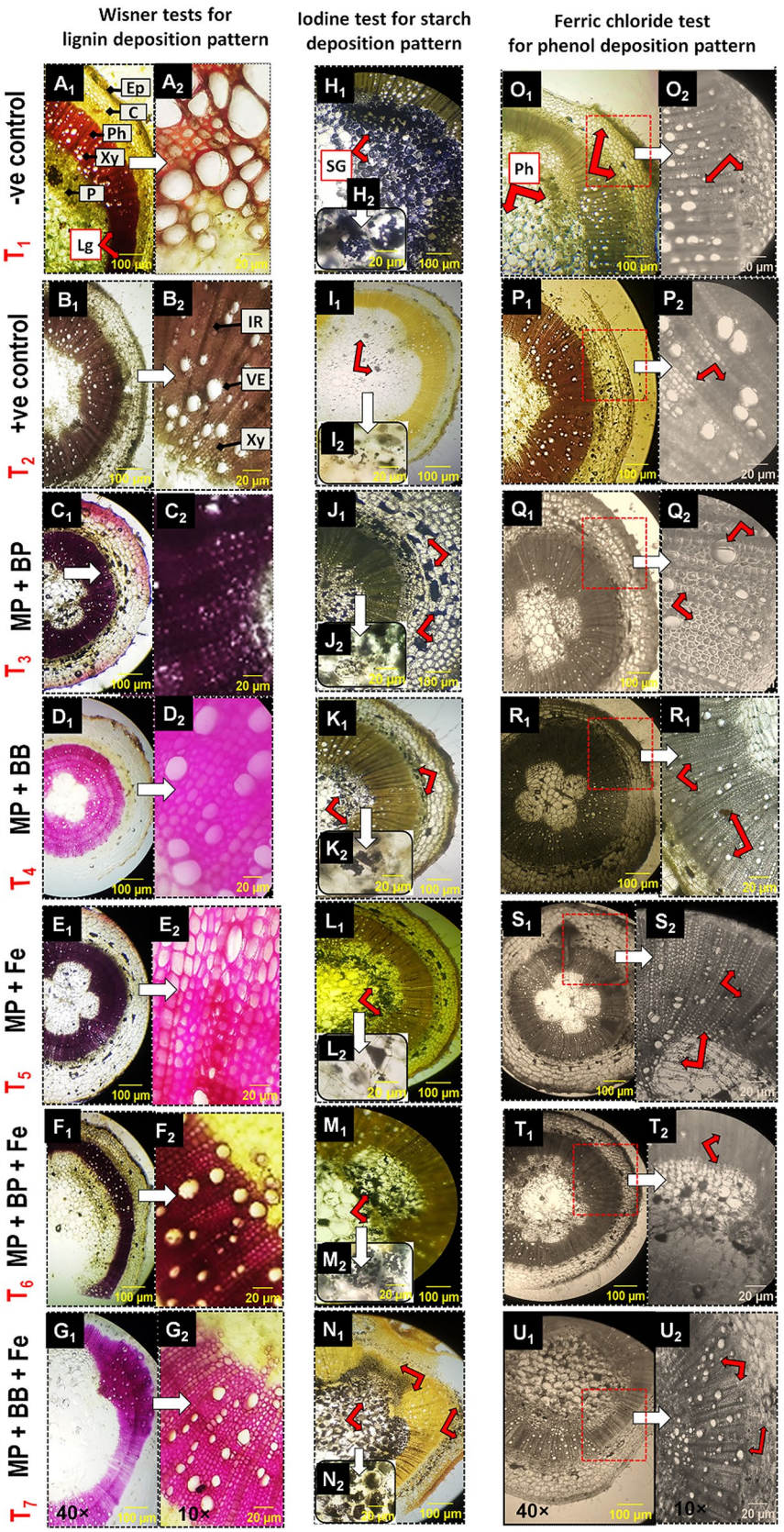

Fig. 14 Effect of *Pseudomonas chlororaphis* subsp. *chlororaphis* (PCC-01) and iron (Fe) on lignin, starch and phenol deposition in the stem of 40-day-old *Solanum lycopersicum* plants under *Macrophomina phaseolina* (MP) stress. Hand-cut cross-sections of the stem at ×10 and ×40. Wisner reagent showing red (**A**, **B**) to pink (**C**–**G**) staining due to the presence of *p*-hydroxycinnamic aldehyde end groups. Potassium iodide reagents for detecting starch showing maximum starch deposition in **J**, **M**, and **N**, moderate in **H**, **K**, and **L**, and less in B. Ferric chloride showing black staining due to deposition of abundant phenols in **Q**–**T** and less in **P**. (**A** −ve control; **B** + ve control (MP only); **C** MP + BP; **D** MP + BB; **E** MP + Fe; **F** MP + Fe-BP; **G** MP + Fe-BB. BP and BB stand for bacterial pellet and bacterial beads, respectively). *Ep* Epidermis, *C* cortex, *Ph* phloem, *Xy* xylem, *P* pith, *IF* interfascicular region, *VE* vessel elements

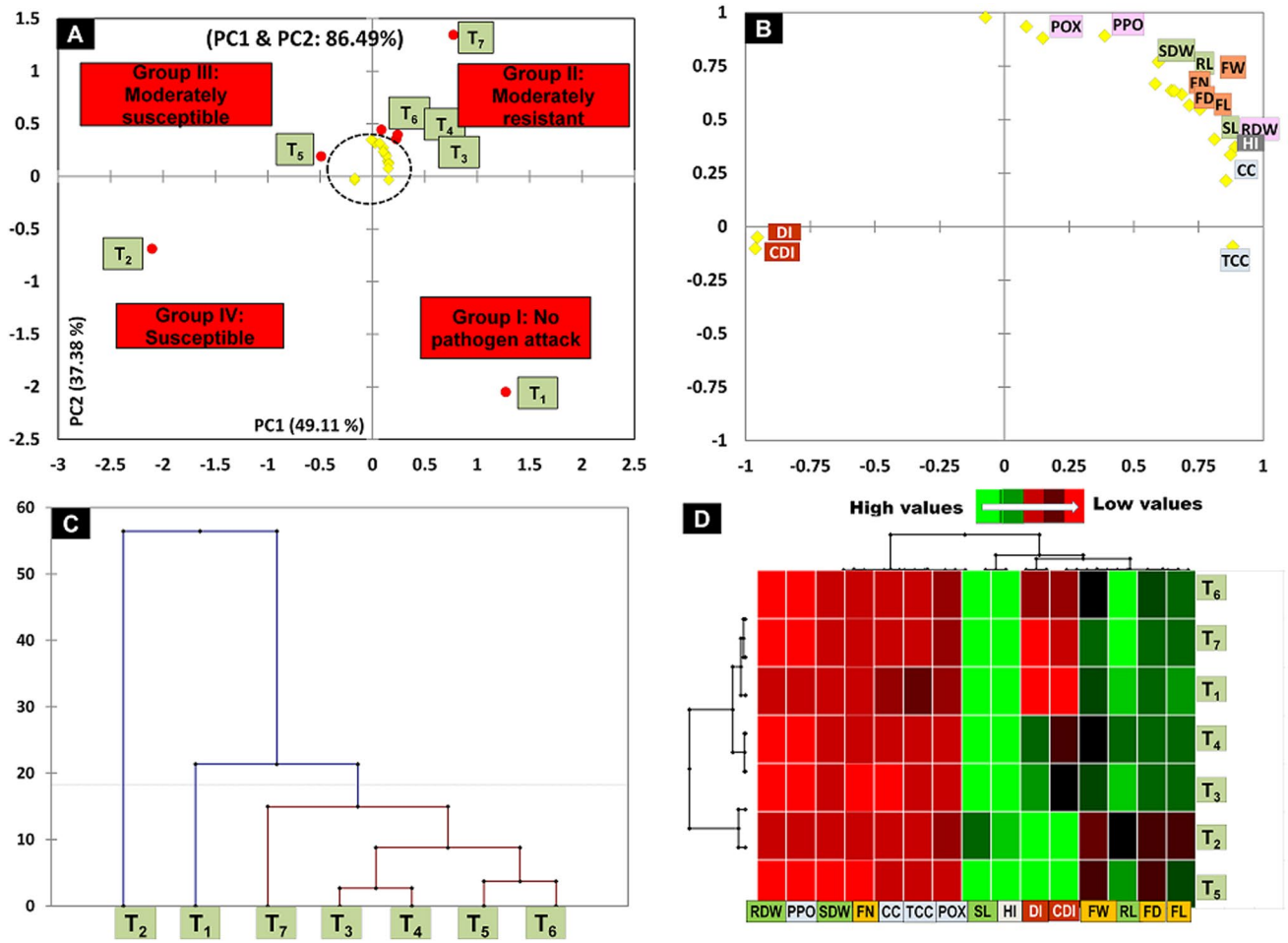

Fig. 15 **A–D** Principal component (**A** and **B**), cluster (**C**), and heat map (**D**) analyses based on disease (maroon), biophysical (green), yield (orange), biochemical (purple and blue), and economics indices (gray) of *Solanum lycopersicum* as affected by charcoal rot disease caused by *Macrophomina phaseolina* (MP). *DI* disease incidence, *DSI* disease severity index, *SL* shoot length, *SFW* shoot fresh weight, *SDW* shoot dry weight, *RL* root length, *RFW* root fresh weight, *RDW* root dry weight, *FN* fruit number, *FW* fruit weight, *FD* fruit diameter, *FL* fruit length, *TCC* total chlorophyll content, *CR* carotenoids, *POX* peroxidase, *PPO* polyphenol oxidase, *PAL* phenylalanine ammonia-lyase

and physio-chemical, attributes (Fig. 15C). These results revealed that the application of Fe-supplemented bacterial beads was a very effective treatment to be used for managing charcoal rot disease in *S. lycopersicum* plants and to obtain higher yield.

Discussion

Pathogenicity of *M. phaseolina*

M. phaseolina was highly virulent on tomato fruit as fruits appeared soft and decayed while showing a 100% infected area on the 20th day after inoculation. By looking at disease symptoms, colony morphology, hyphae, and sclerotia, the fungus was recognized as *Macrophomina phaseolina* (Tassi) Goid. (Hyder et al. 2022).

Characterization of Potential Biocontrol Strain

Further examination of PCC-01 confirmed the positive reaction to IAA, HCN, and the potential to solubilize Fe in accordance with the earlier reports which regarded characteristic features of *P. chlororaphis* for the production of IAA, HCN and for the solubilization of iron along with strong antifungal activity (Mehnaz et al. 2013; Shahid et al. 2017). Many bacteria, including *Pseudomonas*, possess Mn-solubilizing potential via the protonation of metal anions and the synthesis of organic acids that results in a soluble complex of Mn ligands (Ijaz et al. 2021). The elevated growth rate of *P. fluorescens* in a medium supplemented

with $FeCl_2$ or $FeCl_3$ can be attributed to the essential role of Fe as a cofactor in many enzymes of energy metabolism and the occurrence of genes encoding for iron metabolism and homeostasis (e.g., siderophore biosynthesis; Lim et al. 2012). Regarding vigorous antifungal activity against *M. phaseolina* and positive reaction to IAA, HCN, phosphate, and minerals (Fe, Mn, and Zn) solubilization, PCC-01 was ascertained as a potential candidate to be formed as a bioagent for the control of charcoal rot disease in tomato plants caused by *M. phaseolina.* Therefore, the study was extended to prepare alginate beads of PCC-01 as an efficient way for soil inoculation that would maintain bacterial viability and effectiveness (Souza-Alonso et al. 2021).

Characterization of Alginate Beads of PCC-01

Alginate beads of PCC-01 were prepared using sodium alginate solution (2%), as alginate has been proven the most widely used biopolymer for encapsulation, due to its suitability for all types of microorganisms, cost-effective, convenient to execute, and harmless (Rojas-Padilla et al. 2022). FTIR analysis confirmed the association of the PCC-01 within the alginate beads as revealed by variations in the width and frequency of the peaks at the protein region (1600–1200 cm^{-1}) because of crystallinity changes and electrostatic contact between the carboxyl group of sodium alginate with the positive charge of PCC-01 (Adzmi et al. 2012). The UV–vis spectroscopy profiles obtained from pellet and alginate beads of PCC-01 displayed PCC-01 was successfully loaded in alginate; it revealed the same highest absorbance peak at 235 nm without peak dislocation. There was no significant change in the absorbance pattern (200–900 nm), despite the fact that bacterial beads had lower absorbance than bacterial pellets, which can be attributed to changes in the surface morphology of bacterial beads following alginate modification (Tufail et al. 2022).

Alginate beads (PCC-01) have a high encapsulation efficiency (96.20%) because of the thick coating of alginate wall materials surrounding the bacterial cells (Moradi-Pour et al. 2021). The quantity of water absorbed and lost from microcapsules is determined by the parameters like moisture content (93.14%) and swelling ratio (66.14%) (Moradi-Pour et al. 2022). The swelling ratio of bacterial beads occurs due to filling spaces in the beads with alginate, which may result from the presence of more hydrophobic chains (Feng et al. 2019). The alginate beads of PCC-01 were spherical in shape and translucent, with average wet and dry particle sizes of 3.31 mm and 2.70 mm, respectively. The size of the beads has a direct relation to its work efficiency, a diameter of 2–3 mm provides for optimal activity of the immobilized microorganisms since adequate pore size is required for proper nutrient transport inside the matrix (Riaz et al. 2023).

As predicted, the vitality of PCC-01 confined in the alginate matrix reduced a little toward the end of the experiment. The release rate of bacteria from the bead remained the same ($OD_{600} = 2.01$) after the 30th day and then decreased significantly by 18, 40, and 87%, after 60, 90, and 120 days, respectively. The results were in uniformity with previous observations (Souza-Alonso et al. 2021). For example, the concentration of encapsulated *Azospirillum brasilense* remained constant for the first month, reduced by 5% after 3 months, and collapsed by 76% after 7 months of storage at room temperature (Gonzalez et al. 2018). Alginate was thus a suitable carrier for PCC-01 storage in this investigation since it met the three basic conditions for being considered a good matrix (Bashan et al. 2014): (i) aided bacterial strain growth; (ii) maintained a sufficient number of viable cells for a reasonable duration of time; and (iii) injected enough microorganisms to attain a threshold number of bacteria. The film-forming period for the formation of an intact membrane of alginate bacteria was 48 h. All of the above characteristics contribute to make this a suitable formulation for a bacterial cell protector and a stable microenvironment.

In Planta Bioassays

There was a clear separation between the control group (T_1) and the treatment groups ranging from susceptible (T_2), moderately susceptible (T_5), moderately resistant (T_3, T_4, and T_6), and resistant (T_7) with rates of disease severity index 3–75%.

Disease

Typical symptoms of charcoal rot disease (stem blackening, leaf chlorosis, and reduced leaf area) were observed 90 days after transplantation by the end of April. Similar to these results, an absence of charcoal rot disease signs was recorded during the cold season, the early portion of the growing season. However, as the temperature warmed, the symptoms became more obvious with crop maturity till blooming, fruit set, and rising fruit load (Cohen et al. 2022). Charcoal rot disease symptoms such as stem browning, leave yellowing, and wilting occurred on the tomato plants growing in the field during the warm season (Pickel et al. 2020; Hyder et al. 2018).

All treatments (T_3–T_7) significantly managed charcoal rot disease in tomato plants, while the disease was managed more effectively by 90% in T_7 followed by 80% in T_6, 68% in T_4, 65% in T_3, and 30% in T_5. The role of PCC-01 asides from its capability in mineral nutrient utilization and antifungal potential has been attributed to being able to provide systemic resistance in disease management (Xu et al. 2021). The results were consistent with diverse studies describing 80–100% reduction in the charcoal rot disease with *P.*

aeruginosa in soybeans (Ehteshamul-Haque et al. 2007); *P. plecoglossicida* in sorghum (Gopalakrishnan et al. 2011); and *P. fluorescens* alone and in combination with *B. subtilis* in soybeans (Simonetti et al. 2015).

Growth, Biomass, and Yield Indices

Charcoal rot disease in T_2 significantly decreased growth, yield, and harvest index as compared to T_1. Similar results in these attributes occur in many other plants due to the negative consequences of *M. phaseolina* (Shoaib et al. 2018, 2020, 2022). The growth and yield improved variably in different treatments (T_3–T_7), which also improved 'A: B' grade tomatoes as compared to T_2. The economic analysis gave the maximum harvest index in T_7, followed by in T_3, T_4, T_5, and T_6. Promising consequences with alginate beads of PCC-01 along with Fe particularly in T_7 as revealed by multivariate analysis might be linked with the slow release of bacteria from the beads and their potential to survive in the root compartment for a prolonged period. Other PGPR strains had a beneficial initial root colonization rate that gradually reduced in the latter phases of plant development (Bertani et al. 2021). Addition benefits in terms of harvest index in T_7 could be correlated with the potential of fluorescent *Pseudomonads* to produce Fe chelating compounds that may contribute to plant nutrition under limiting conditions (Bar-Ness et al. 1992; Shirley et al. 2011).

Physiology and Histo-chemistry

The observations on physicochemical, histo-chemical, and gene expression were in accordance with the biophysical attributes of the tomato plants. There was a reduction in the physicochemical attributes like photosynthetic pigments and antioxidant enzymes (POX, PPO, and PAL) in T_2 as compared to T_1. *M. phaseolina* has the ability to hold onto the host tissues by cellulose-binding elicitor and lectins, which overcome the initial host defense and penetrate the plant epidermis through the production of different kinds of toxic chemicals and cell wall-damaging enzymes that alter the host defense mechanism (Shoaib et al. 2022). Disturbance in the physicochemical attributes of the plants in T_2 might result from the hijacking plant defense system by the *M. phaseolina* through induction of oxidative stress (Khan et al. 2018; Marquez et al. 2021; Shoaib et al. 2021). Histochemical analysis explored the damaged epidermis, cortex, and pith region with less deposition of lignin, phenolics, and starch in T_2 (Hemmati et al. 2018).

There was substantial enhancement in the total chlorophyll content and carotenoids in different treatments (T_3–T_7) as compared to T_2. This could be due to increase in the photosynthetic leaf area of plants by the action of PCC-01 and Fe (Awan et al. 2022, 2023). Likewise, the activity of POX, PPO, and PAL improved, with the maximum activity being recorded in T_7, followed by T_6, T_5, T_4, and T_3 in comparison to T_2. In addition to a pathogen attack, beneficial microorganisms trigger several types of defensive enzymes in host plants (Awan et al. 2022). POX as a heme-containing antioxidative enzyme contributes substantially to the polymerization of lignin through the phenylpropanoid pathway (Shoaib et al. 2021). PPO is a copper-containing functional enzyme that hydroxylates and oxidizes phenolic substances to produce highly reactive ortho-quinones with anti-pathogenic effects (Li and Steffens 2002). PAL catalyzes the initial step in the phenylpropanoid pathway, the conversion of L-phenylalanine to trans-cinnamic acid, resulting in the synthesis of phytoalexins and phenolic compounds. Therefore, enhanced activation of POX, PPO, and PAL indicated that the enzymes can be induced by the bacterium or pathogen, and may prevent *M. phaseolina* infection in tomato plants through enhanced production of phenols and lignin (Shoaib et al. 2021).

The results on biochemical attributes were supported by the histo-chemical analysis. Thus, the accumulation patterns of phenols, lignin, and starch granules were greater in T_3–T_7 in comparison to T_2, which not only strengthened cell walls during pathogen penetration but also induce the accumulation of anthocyanins and other antioxidants to act as a protective shield against pathogen-induced oxidative stress (Lochman et al. 2020). The thickness, toughness, and mechanical strength of the lignified cell wall could protect the differentiated cells, reduce cell gap, and hence induce resistance to pathogen infection (Yang et al. 2018).

Conclusions

Phytopathogenic fungus, *M. phaseolina*, was highly virulent on tomato fruit causing 100% infection in 20 days after inoculation. Screening trial showed the highest antifungal activity of 71% by *P. chlororaphis* subsp. *chlororaphis* (PCC-01) against *M. phaseolina* followed by 64, 61, and 57% by *P. chlororaphis* subsp. *aurantiaca* (PCA-02), *B. amyloliquefaciens* (BA-01), and *P. aurantiaca* (PA-03), respectively. PCC-01 confirmed the positive reaction to IAA and HCN, along with the potential to solubilize phosphate and iron. PCC-01 was successfully loaded in alginate beads, as indicated by FTIR [altered peak areas intensity at the protein region (1600–1200 cm^{-1})] and UV–vis (maximum absorbance peak at $\cong$235 nm without peak dislocation) analysis. The alginate beads of PCC-01 were spherical (wet size 3.31 and dry size 2.70 mm) with encapsulation efficiency higher than 95%, swelling ratio (66.47%), moisture content (92.50%), film-forming time (48 h), and slow release of entrapped bacteria till 120 days. In planta, multivariate analysis with all 18 traits including disease, morph growth,

yield, biochemical, and gene expression-related indices of tomato plants verified the greater disease-managing potential of alginate beads of Fe-amended PCC-01 through maximum economic returns. As a disease management approach, the alginate beads of PCC-01 in the presence of Fe could be a successful strategy to provide high crop yields, good crop quality, and a profit margin to the end-users. In addition to promoting plant development, PCC-01 can prevent plant diseases by generating such substances that have a toxic effect to pathogens and stimulating the plant immune system by up-regulating antioxidant machinery.

Future Prospective

Iron-amended alginate beads of *P. chlororaphis* subsp. *chlororaphis* (PCC-01) is a promising agricultural option that enhances the utilization of microbial inoculants through slow-release strategy. In vitro and in planta data indicated that PCC-01 together with Fe has the potential to be developed as a commercial bioagent for the control of charcoal rot in tomatoes, an emerging threat in tomato production increased by a lack of registered fungicides and resistant varieties against the pathogen *M. phaseolina*. Different formulations of PCC-01 and Fe might be developed and commercialized as a single-source solution for sustainable and highly profitable tomato crop production.

Author Contributions Amna Shoaib: conceptualization, supervision, acquisition, analysis, interpretation of data for the work, drafting the manuscript, and producing the figures; Huma Shafique: experiment and data curation; Aneela Anwar: acquisition and analysis; Sidrah Javed: anatomy and coordinated the work; Barizah Malik: acquisition and analysis; Samina Mehnaz: characterized, identified, and provided bacterial cultures.

Declarations

Conflict of Interest The authors declare that they have no known competing financial interests or personal relationships that could have appeared to influence the work reported in this paper.

References

Adhikary NK, Chowdhury MR, Begum T, Mallick R (2019) Integrated management of stem and root rot of sesame (*Sesamum indicum* L.) caused by *Macrophomina phaseolina* (Tassi) Goid. Int J Curr Microbiol Appl Sci 8:22–24

Adzmi F, Meon S, Musa MH, Yusuf NA (2012) Preparation, characterisation and viability of encapsulated *Trichoderma harzianum* UPM40 in alginate-montmorillonite clay. J Microencapsul 29:205–210

Akhtar S, Shoaib A, Javiad I, Qaisar U, Tasadduq R (2023) Farmyard manure, a potential organic additive to reclaim copper and *Macrophomina phaseolina* stress responses in mash bean plants. Sci Rep 13:14383

Arrebola E, Tienda S, Vida C, de Vicente A, Cazorla FM (2019) Fitness features involved in the biocontrol interaction of *Pseudomonas chlororaphis* with host plants: the case study of PcPCL1606. Front Microbiol 10:719

Awan ZA, Shoaib A, Iftikhar MS, Jan BL, Ahmad P (2022) Combining biocontrol agents with plant nutrients for integrated control of tomato early blight through modulation of physic-chemical attributes and key oxidants. Front Microbiol 13:807699

Awan ZA, Shoaib A, Schenk PM, Ahmad A, Alansi S, Paray BA (2023) Antifungal potential of volatiles produced by *Bacillus subtilis* BS-01 against *Alternaria solani* in *Solanum lycopersicum*. Front Plant Sci 13:1089562

Bar-Ness E, Hadar Y, Chen Y, Shanzer A, Libman J (1992) Iron uptake by plants from microbial siderophores: a study with 7-nitrobenz-2 oxa-1, 3-diazole-desferrioxamine as fluorescent ferrioxamine B analog. Plant Physiol 99:1329–1335

Bashan Y, de-Bashan LE, Prabhu SR, Hernandez JP (2014) Advances in plant growth-promoting bacterial inoculant technology: formulations and practical perspectives (1998–2013). Plant Soil 378:1–33

Bertani I, Zampieri E, Bez C, Volante A, Venturi V, Monaco S (2021) Isolation and characterization of *Pseudomonas chlororaphis* strain ST9; rhizomicrobiota and in planta studies. Plants 10:1466

Cohen R, Elkabetz M, Paris HS, Gur A, Dai N, Rabinovitz O, Freeman S (2022) Occurrence of *Macrophomina phaseolina* in Israel: challenges for disease management and crop germplasm enhancement. Plant Dis 106:15–25

Ehteshamul-Haque S, Sultana V, Ara J, Athar M (2007) Cultivar response against root-infecting fungi and efficacy of *Pseudomonas aeruginosa* in controlling soybean root rot. Plant Biosyst 141:51–55

FAOSTAT (2023) Food and agriculture organization corporate statistical database. https://www.fao.org/faostat/en/#home

Fathi F, Saberi Riseh R, Khodaygan P, Hosseini S, Skorik YA (2021) Microencapsulation of a *Pseudomonas* strain (VUPF506) in alginate–whey protein–carbon nanotubes and next-generation sequencing identification of this strain. Polymers 13:4269

Feng J, Dou J, Wu Z, Yin D, Wu W (2019) Controlled release of biological control agents for preventing aflatoxin contamination from starch–alginate beads. Molecules 24:1858

Gonzalez EJ, Hernandez JP, de-Bashan LE, Bashan Y (2018) Dry micro-polymeric inoculant of *Azospirillum brasilense* is useful for producing mesquite transplants for reforestation of degraded arid zones. Appl Soil Ecol 129:84–93

Gopalakrishnan S, Humayun P, Kiran BK, Kannan IGK, Vidya MS, Deepthi K, Rupela O (2011) Evaluation of bacteria isolated from rice rhizosphere for biological control of charcoal rot of sorghum caused by *Macrophomina phaseolina* (Tassi) Goid. World J Microbiol Biotechnol 27:1313–1321

Hemmati P, Zafari D, Mahmoodi SB, Hashemi M, Gholamhoseini M, Dolatabadian A, Ataei R (2018) Histopathology of charcoal rot disease (*Macrophomina phaseolina*) in resistant and susceptible cultivars of soybean. Rhizosphere 7:27–34

Hyder S, Gondal AS, Ahmed R, Sahi ST, Rehman A, Hannan A (2018) First report of charcoal rot in tomato caused by *Macrophomina phaseolina* (Tassi) Goid. from Pakistan. Plant Dis 102:1459

Hyder S, Gondal AS, Rizvi ZF, Iqbal R, Hannan A, Sahi ST (2022) Antagonism of selected fungal species against *Macrophomina phaseolina* (Tassi) goid, causing charcoal rot of Mungbean. Pak J Bot 54:1129–1138

Ijaz A, Mumtaz MZ, Wang X, Ahmad M, Saqib M, Maqbool H, Mustafa A (2021) Insights into manganese solubilizing *Bacillus*

spp. for improving plant growth and manganese uptake in maize. Front Plant Sci 12:719504

Khan KA, Shoaib A, Awan ZA, Basit A, Hussain M (2018) *Macrophomina phaseolina* alters biochemical pathway in *Vigna radiata* that is chastened by Zn and FYM to improve plant growth. J Plant Interact 13:131–140

Kotasthane AS, Agrawal T, Zaidi NW, Singh US (2017) Identification of siderophore producing and cynogenic *Pseudomonas fluorescent* and a simple confrontation assay to identify potential bio-control agent for collar rot of chickpea. 3 Biotech 7:137

Kumar A, Jindal SK, Dhaliwal MS, Sharma A, Kaur S, Jain S (2019) Gene pyramiding for elite tomato genotypes against ToLCV (*Begomovirus* spp.), late blight (*Phytophthora infestans*) and RKN (*Meloidogyne* spp.) for northern India farmers. Physiol Mol Biol Plants 25:1197–1209

Li L, Steffens JC (2002) Overexpression of polyphenol oxidase in transgenic tomato plants results in enhanced bacterial disease resistance. Planta 215:239–247

Lim CK, Hassan KA, Tetu SG, Loper JE, Paulsen IT (2012) The effect of iron limitation on the transcriptome and proteome of *Pseudomonas fluorescens* Pf-5. PLoS ONE 7:e39139

Lochman J, Dadáková K, Heinrichová T, Kašparovský T (2020) Production of defense phenolics in tomato leaves of different age. Molecule 25:4952

Lokesh R, Rakholiya KB, Thesiya MR (2020) Evaluation of different fungicides against *Macrophomina phaseolina* (Tassi) Goid. causing dry root rot of chickpea (*Cicer arietinum* L.) *in vitro*. Int J Curr Microbiol Appl Sci 9:901–911

Ma L, Terwilliger A, Maresso AW (2015) Iron and zinc exploitation during bacterial pathogenesis. Metallomics 7:1541–1554

Marquez N, Giachero ML, Declerck S, Ducasse DA (2021) *Macrophomina phaseolina*: general characteristics of pathogenicity and methods of control. Front Plant Sci 12:634397

Mehnaz S, Saleem RSZ, Yameen B, Pianet I, Schnakenburg G, Pietraszkiewicz H, Gross H (2013) Lahorenoic acids A-C, orthodialkyl-substituted aromatic acids from the biocontrol strain *Pseudomonas aurantiaca* PB-St2. J Nat Prod 76:135–141

Moradi-Pour M, Saberi-Riseh R, Esmaeilzadeh-Salestani K, Mohammadinejad R, Loit E (2021) Evaluation of *Bacillus velezensis* for biological control of *Rhizoctonia solani* in bean by alginate/gelatin encapsulation supplemented with nanoparticles. Microbiol BioTechnol 31:1373–1382

Moradi-Pour M, Saberi Riseh R, Ranjbar-Karimi R, Hassanisaadi M, Rahdar A, Baino F (2022) Microencapsulation of *Bacillus velezensis* using alginate-gum polymers enriched with TiO_2 and SiO_2 nanoparticles. Micromachines 13:1423

Nafisa, Shoaib A, Iqbal J, Khan KA (2020) Evaluation of phenotypic, physiological and biochemical attributes connected with resistance in tomato against *Alternaria solani*. Acta Physiol Plant 42:1–7

Nithyapriya S, Lalitha S, Sayyed RZ, Reddy MS, Dailin DJ, El-Enshasy HA, Luh Suriani N, Herlambang S (2021) Production, purification, and characterization of bacillibactin siderophore of *Bacillus subtilis* and its application for improvement in plant growth and oil content in sesame. Sustainability 13:5394

Nizam A, Thattantavide A, Kumar A (2023) Gene expression pattern, lignin deposition and root cell wall modification of developing mangrove propagules under salinity stress. J Plant Growth Regul 22:1–7

Patten CL, Glick BR (1996) Bacterial biosynthesis of indole-3-acetic acid. Can J Microbiol 42:207–220

Pickel B, Dai N, Maymon M, Elazar M, Tanami Z, Frenkel O, Freeman S (2020) Development of a reliable screening technique for determining tolerance to *Macrophomina phaseolina* in strawberry. Eur J Plant Pathol 157:707–718

Riaz G, Shoaib A, Javed S, Perveen S, Ahmed W, El-Sheikh MA, Kaushik P (2023) Formulation of the encapsulated rhizospheric *Ochrobactrum ciceri* supplemented with alginate for potential antifungal activity against the chili collar rot pathogen. S Afr J Bot 161:586–598

Riseh RS, Hassanisaadi M, Vatankhah M, Kennedy JF (2022) Encapsulating biocontrol bacteria with starch as a safe and edible biopolymer to alleviate plant diseases: a review. Carbohydr Polym 302:120384

Rizwana H, Bokahri NA, Alsahli SA, Al Showiman AS, Alzahrani RM, Aldehaish HA (2021) Postharvest disease management of Alternaria spots on tomato fruit by *Annona muricata* fruit extracts. Saudi J Biol Sci 28:2236–2244

Rojas-Padilla J, De-Bashan LE, Parra-Cota FI, Rocha-Estrada J, de Los Santos-Villalobos S (2022) Microencapsulation of Strains for improving wheat (*Triticum turgidum* Subsp. durum) growth *Bacillus* and development. Plants 11:2920

Rout GR, Sahoo S (2015) Role of iron in plant growth and metabolism. Rev Agric Sci 3:1–24

Rovera M, Pastor N, Niederhauser M, Rosas SB (2014) Evaluation of *Pseudomonas chlororaphis* subsp. *aurantiaca* SR1 for growth promotion of soybean and for control of *Macrophomina phaseolina*. Biocontrol Sci Technol 24:1012–1025

Saarai A, Kasparkova V, Sedlacek T, Sáha P (2013) On the development and characterisation of crosslinked sodium alginate/gelatine hydrogels. J Mech Behav Biomed Mater 18:152–166

Safari MR, Farokhzad M, Kaviani B, Kulus D (2022) Endophytic fungi as potential biocontrol agents against *Sclerotium rolfsii* sacc. the causal agent of peanut white stem rot disease. Cells 11:2643

Schaker PD, Peters LP, Cataldi TR, Labate CA, Caldana C, Monteiro-Vitorello CB (2017) Metabolome dynamics of smutted sugarcane reveals mechanisms involved in disease progression and whip emission. Front Plant Sci 8:264892

Schmidt W, Thomine S, Buckhout TJ (2020) Iron nutrition and interactions in plants. Front Plant Sci 10:1670

Shahid I, Rizwan M, Baig DN, Saleem RS, Malik KA, Mehnaz S (2017) Secondary metabolites production and plant growth promotion by *Pseudomonas chlororaphis* subsp. *aurantiaca* strains isolated from cotton, cactus, and para grass. J Microbiol Biotechnol 27:480–491

Shahid I, Han J, Hardie D, Baig DN, Malik KA, Borchers CH, Mehnaz S (2021a) Profiling of antimicrobial metabolites of plant growth promoting *Pseudomonas* spp. isolated from different plant hosts. 3 Biotech 11:48

Shahid I, Han J, Hanooq S, Malik KA, Borchers CH, Mehnaz S (2021b) Profiling of metabolites of *Bacillus* spp. and their application in sustainable plant growth promotion and biocontrol. Front Sustain Food Syst 5:605195

Shcherbakova LA, Nazarova TA, Mikityuk OD, Istomina EA, Odintsova TI (2018) An extract purified from the mycelium of a tomato wilt-controlling strain of *Fusarium sambucinum* can protect wheat against *Fusarium* and common root rots. Pathogens 7:61

Shirley M, Avoscan L, Bernaud E, Vansuyt G, Lemanceau P (2011) Comparison of iron acquisition from Fe–pyoverdine by strategy I and strategy II plants. Botany 89:731–735

Shoaib A, Munir M, Javaid A, Awan ZA, Rafiq M (2018) Anti-mycotic potential of *Trichoderma* spp. and leaf biomass of *Azadirachta indica* against the charcoal rot pathogen, *Macrophomina phaseolina* (Tassi) Goid in cowpea. Egypt J Biol Pest Control 28:26

Shoaib A, Ali H, Javaid A, Awan ZA (2020) Contending charcoal rot disease of mungbean by employing biocontrol *Ochrobactrum ciceri* and zinc. Physiol Mol Biol Plants 26:1385–1397

Shoaib A, Ferdosi MFH, Saleem A, Javed S (2021) Morphological and biochemical variations induced by synergy of salicylic acid and zinc in cockscomb. Folia Hortic 33:1–11

Shoaib A, Abbas S, Nisar Z, Javaid A, Javed S (2022) Zinc highly potentiates the plant defense responses against *Macrophomina phaseolina* in mungbean. Acta Physiol Plant 44:1–17

Siddique S, Shoaib A, Khan SN, Mohy-Ud-Din A (2021) Screening and histopathological characterization of sunflower germplasm for resistance to *Macrophomina phaseolina*. Mycologia 113(1):92–107

Simonetti E, Viso NP, Montecchia M, Zilli C, Balestrasse K, Carmona M (2015) Evaluation of native bacteria and manganese phosphite for alternative control of charcoal root rot of soybean. Microbiol Res 180:40–48

Souza-Alonso P, Rocha M, Rocha I, Ma Y, Freitas H, Oliveira RS (2021) Encapsulation of *Pseudomonas libanensis* in alginate beads to sustain bacterial viability and inoculation of *Vigna unguiculata* under drought stress. 3 Biotech 11:293

Tirry N, Ferioun M, Laghmari G, Kouchou A, Bahafid W, El B (2022) Effect of co-immobilized tri-bacteria into alginate beads on growth and root mycorrhizal colonization potential of *Medicago sativa* plants. Biointerface Res Appl Chem 13:451

Tufail MS, Liaqat I, Andleeb S, Naseem S, Zafar U, Sadiqa A, Saleem G (2022) Biogenic synthesis, characterization and antibacterial properties of silver nanoparticles against human pathogens. J Oleo Sci 71:257–265

Xu W, Xu L, Deng X, Goodwin PH, Xia M, Zhang J, Yang L (2021) Biological control of take-all and growth promotion in wheat by *Pseudomonas chlororaphis* YB-10. Pathogens 10:903

Yang C, Liang Y, Qiu D, Zeng H, Yuan J, Yang X (2018) Lignin metabolism involves *Botrytis cinerea* BcGs1-induced defense response in tomato. BMC Plant Biol 18:1–15

Yaqoob HS, Shoaib A, Anwar A, Perveen S, Javed S, Mehnaz S (2024) Seed biopriming with *Ochrobactrum ciceri* mediated defense responses in *Zea mays* (L.) against *Fusarium* rot. Physiol Mol Biol Plant 30:49–66